https://doi.org/10.5194/essd-2026-704
Preprint. Discussion started: 16 November 2026
© Author(s) 2026. CC BY 4.0 License.



Open Access Earth System Science Data Discussions

ChinaMet: A multisource integrated high-resolution multi-variable meteorological dataset for China

Yingyi Hu[1,2], Ling Zhang[1]*, Yanbo Zhao[1], Tao Che[1]

[1]Key Laboratory of Remote Sensing of Gansu Province, Heihe Remote Sensing Experimental Research Station, Northwest Institute of Eco-Environment and Resources, Chinese Academy of Sciences, Lanzhou 730000, China
[2]School of Earth System Science, Tianjin University, Tianjin 300072, China

Correspondence to: Ling Zhang (zhanglingky@lzb.ac.cn)

Abstract. High-quality meteorological forcing data are essential for hydrological modelling, climate-impact assessment, ecological analysis, and land-surface process studies. However, existing meteorological datasets for China remain limited by variable completeness, spatial resolution, temporal continuity, and performance in topographically complex and observation-sparse regions. Here, we present ChinaMet, a multisource integrated, high-resolution, multi-variable meteorological dataset for China spanning 1980–2024. ChinaMet integrates observations from more than 2,300 meteorological stations with satellite products, reanalysis data, and topographic covariates, and provides daily, monthly, and annual fields of precipitation, 2-m mean, maximum, and minimum air temperature, 10-m wind speed, relative humidity, surface pressure, and potential evapotranspiration at 0.01° (~1 km) resolution. ChinaMet was produced using a computationally efficient merging–downscaling framework, in which multisource meteorological information is first merged at 0.1° using random forest models and subsequently downscaled to 0.01° using climatologically aided interpolation. To improve estimates in regions with sparse or no station observations, particularly over the Tibetan Plateau, ERA5-Land-derived virtual stations were introduced to constrain spatial extrapolation and reduce systematic biases. ChinaMet was evaluated against independent station observations, prefecture-level precipitation statistics from water resources bulletins, national precipitation records, and several widely used meteorological products. For precipitation, ChinaMet closely reproduced station-based annual means and achieved the best overall agreement at the prefecture scale (R^2 = 0.92, RMSE = 177 mm, Bias = −26 mm), with 85% agreement in precipitation trend direction. ChinaMet also consistently reproduced spatial temperature patterns, while Three-Cornered Hat analysis indicated the lowest monthly uncertainty among the evaluated products for both precipitation (8.2 mm month^{-1}) and mean air temperature (0.36 °C). ChinaMet provides a spatially detailed, temporally continuous, and internally consistent meteorological forcing dataset for hydrological, ecological, agricultural, and climate-related applications across China. The dataset is openly available from the National Cryosphere Desert Data Center at https://doi.org/10.12072/ncdc.nieer.db6722.2025 (Zhang et al., 2025).

https://doi.org/10.5194/essd-2026-704
Preprint. Discussion started: 16 November 2026
© Author(s) 2026. CC BY 4.0 License.



Open Access Earth System Science Data Discussions

1 Introduction

Meteorological forcing data are fundamental inputs for hydrological and water resources studies, eco-environmental modeling, and land surface process analyses, and they directly affect the accuracy and reliability of numerical simulations (Funk et al., 2015; Gelaro et al., 2017; Tang et al., 2022; Thiemig et al., 2022; Hu et al., 2024). Key meteorological variables, including precipitation, air temperature, wind speed, and air pressure, not only control the simulation of hydrological processes such as surface runoff, soil moisture, and evapotranspiration, but also influence investigations of ecosystem carbon and water cycles, vegetation dynamics, and climate change mechanisms. Therefore, high-quality meteorological forcing data are a prerequisite for understanding climate–ecosystem interactions. However, existing meteorological forcing products do not fully meet the current demand for multiscale and high-accuracy simulations. On the one hand, these products differ substantially in their generation methods and variable completeness, leading to inconsistent performance across regions and time periods. On the other hand, their spatial resolutions are often insufficient for detailed local-scale simulations, particularly in mountainous and arid regions with complex terrain or limited observational data (Mankin et al., 2025).

Currently, multivariable meteorological forcing products are primarily derived from reanalysis datasets and station observation-based interpolated datasets (Beck et al., 2022). Reanalysis datasets are generated by integrating global or regional numerical weather prediction models with multisource observations through data assimilation systems, and they offer advantages such as strong spatiotemporal continuity and high physical consistency. In recent years, several global reanalysis products have been widely used in hydrological and climate studies, including the Japanese 55-year Reanalysis (JRA-55; Kobayashi et al., 2015), the fifth-generation ECMWF atmospheric reanalysis (ERA5; Hersbach et al., 2020) and its downscaled land component, ERA5-Land (Muñoz-Sabater et al., 2021), and the Global Land Data Assimilation System (GLDAS; Yan et al., 2021). In addition to reanalysis products, station observation-based interpolated datasets improve regional applicability through spatial extrapolation or interpolation techniques, with representative examples including the Global Surface Summary of the Day (GSOD) dataset and WorldClim (Fick and Hijmans, 2017). These global meteorological forcing datasets provide indispensable support for characterizing the complex dynamics of the Earth system, advancing our understanding of the hydrological cycle and land–atmosphere interactions, and supporting research on climate change prediction and its environmental impacts.

Although global reanalysis datasets and station observation-based meteorological forcing products have played an important role in climate research, their spatial resolutions are often insufficient for fine-scale hydrological modeling and extreme weather analysis. A major limitation of reanalysis datasets arises from model errors and uncertainties in data assimilation. Because reanalysis products rely on numerical weather prediction models, limitations in parameterization schemes, terrain representation, and physical process descriptions can lead to estimation biases over complex terrain, during extreme weather events, and at regional scales (Fick and Hijmans, 2017; Amjad et al., 2020; Beck et al., 2020; Jiang et al., 2021; Gomis-Cebolla et al., 2023). For example, ERA5 exhibits systematic biases in precipitation and surface radiative fluxes (Hersbach et al., 2020), while GLDAS shows limited accuracy in simulating soil moisture and evapotranspiration in arid

https://doi.org/10.5194/essd-2026-704
Preprint. Discussion started: 16 November 2026
© Author(s) 2026. CC BY 4.0 License.



regions (Xia et al., 2014). In addition, in regions with sparse observations, reanalysis datasets may fail to accurately capture local meteorological characteristics (Jiang et al., 2023a). Similarly, although station observation-based meteorological forcing products can provide relatively high accuracy at individual stations, their performance is constrained by limited spatial representativeness and interpolation methods, resulting in larger uncertainties in regions with sparse station networks or complex topography (Hofstra et al., 2008). For instance, WorldClim shows reduced temperature interpolation accuracy in regions with sparse meteorological observations (Fick and Hijmans, 2017). Moreover, most interpolation methods, such as inverse distance weighting, kriging, and thin-plate splines, assume smooth spatial variations in meteorological variables and may neglect local climatic processes and small-scale weather systems, thereby affecting the reliability of meteorological forcing data. Overall, both reanalysis datasets and interpolation-based meteorological forcing products suffer from data biases, limited spatial resolution, and insufficient capability in representing extreme weather events.

In recent years, increasing efforts have been made to integrate satellite observations, reanalysis datasets, and ground-based observations using methods such as machine learning, Bayesian merging, and optimal interpolation (OI). These approaches exploit the complementary strengths of different data sources and help alleviate the limitations of single-source datasets in terms of regional applicability and biases in observation-sparse regions (Zhang et al., 2021; Yu et al., 2023; Zhang et al., 2023; Hu and Zhang, 2024). However, most existing studies have focused on the development of products for individual meteorological variables, such as precipitation and air temperature (Supplementary Table S1). High-quality meteorological forcing data require not only high accuracy for individual variables, but also the preservation of covariability among different meteorological variables (Mankin et al., 2025). Such physical consistency is essential for accurately characterizing hydrological cycle processes and their responses to climate change (Fick and Hijmans, 2017; Peng et al., 2019; He et al., 2020; Beck et al., 2022). In addition, fusion algorithms face an inherent trade-off between computational efficiency and improvements in spatiotemporal accuracy, particularly at large spatial scales such as national or global domains. Although high-resolution fused products can provide more detailed representations of land surface characteristics, they are usually associated with substantially increased computational costs. Meanwhile, statistically based fusion techniques may improve processing efficiency, but they may not fully preserve the physical consistency among different data sources and meteorological variables.

China spans the Tibetan Plateau, the eastern monsoon region, and the arid regions of northwestern China, with pronounced topographic heterogeneity and strong climatic gradients. Several meteorological products have been developed for China in recent years (Supplementary Table S1). Most of these products provide basic temperature and precipitation data, but key forcing variables such as wind speed, air pressure, relative humidity, and potential evapotranspiration are often absent. In addition, some existing meteorological forcing products rely on a single data source, commonly station-based interpolation, which can lead to large uncertainties and reduced accuracy in regions with sparse observational networks. Their spatiotemporal resolution and update frequency also remain insufficient to meet the dual requirements of fine-scale modeling and long-term change analysis. In particular, kilometer-scale high-resolution meteorological datasets are still limited for China; most commonly used meteorological forcing products have spatial resolutions of 0.1° or coarser. Moreover, many datasets are

https://doi.org/10.5194/essd-2026-704
Preprint. Discussion started: 16 November 2026
© Author(s) 2026. CC BY 4.0 License.



updated with substantial delays, limiting their timeliness and their applicability for near-real-time data integration and dynamic modeling under a changing climate.

To address the above challenges and limitations, we developed ChinaMet (Zhang et al., 2025), a high-resolution, long-term, multivariable meteorological forcing dataset specifically designed for China. ChinaMet provides daily meteorological forcing data at 1 km spatial resolution for the period 1980–2024. The dataset was generated by integrating satellite observations, reanalysis datasets, and ground-based observations from more than 2,300 meteorological stations. It includes eight variables: precipitation (pre), 2 m mean air temperature (tmpmean), maximum air temperature (tmpmax), minimum air temperature (tmpmin), 10 m wind speed (wind), relative humidity (rhu), surface air pressure (pres), and potential evapotranspiration (pet). Compared with existing meteorological forcing products, ChinaMet makes contributions in both methodological development and dataset characteristics. Methodologically, we adopted a fusion algorithm combined with a statistical downscaling strategy to balance computational efficiency with improved spatiotemporal accuracy. In addition, a virtual-station technique was introduced to improve data representativeness in observation-sparse regions, thereby enhancing the applicability and reliability of the model in these areas. In terms of dataset characteristics, ChinaMet provides a kilometer-scale, daily, multivariable meteorological forcing product covering more than four decades from 1980 to the present. The dataset is publicly available from the National Cryosphere Desert Data Center (https://doi.org/10.12072/ncdc.nieer.db6722.2025). To date, it has been accessed more than 50,000 times and downloaded more than 3,800 times, providing a refined meteorological forcing dataset for hydrometeorological research across China.

2 Data

2.1 Gauge-based observations

The gauge-based observations used in this study were primarily obtained from the China Meteorological Administration (CMA; http://data.cma.cn). The dataset includes observational records from more than 2,300 meteorological stations across mainland China during 1980–2024 (Figure 1a). As shown in Figure 1b and 1c, the meteorological stations are unevenly distributed across China, with most stations concentrated in the mid- to low-latitude regions between 25°N and 40°N and in the longitude range of 90°E–130°E. In contrast, station coverage is relatively sparse in regions with complex terrain, such as the Tibetan Plateau, Xinjiang, and northwestern China (Hu and Zhang, 2024). The daily observations used in this study represent accumulated measurements or mean values over the period from 08:00 to 08:00 Beijing Time (UTC+8), corresponding to 00:00–24:00 UTC. These data have undergone strict quality control procedures (Zhao and Yatagai, 2014), including: (i) manual inspection and correction; (ii) extreme value checks; (iii) spatiotemporal consistency checks; and (iv) internal consistency checks, such as the identification of duplicate records and erroneous units.

https://doi.org/10.5194/essd-2026-704
Preprint. Discussion started: 16 November 2026
© Author(s) 2026. CC BY 4.0 License.

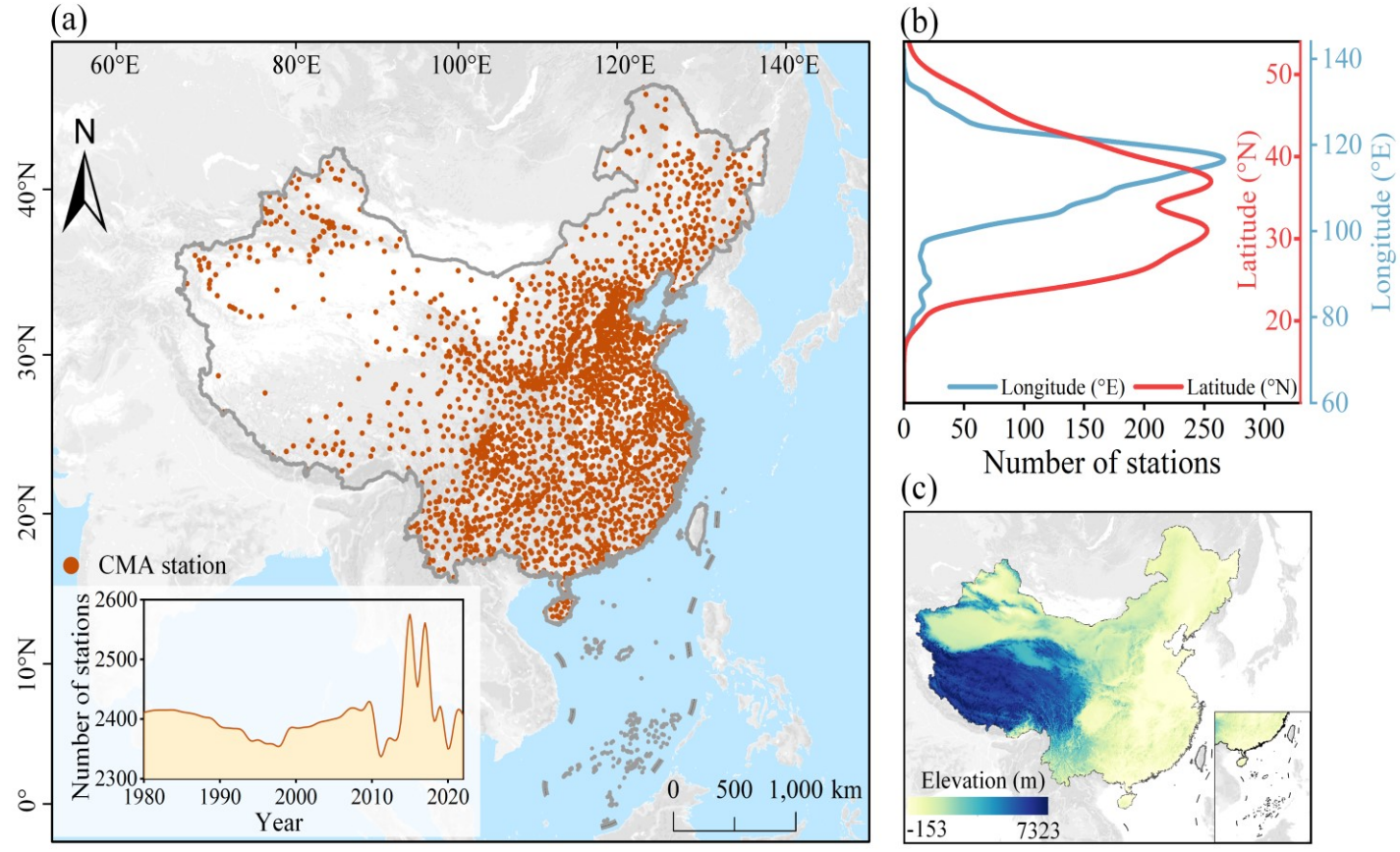


Figure 1. Study area. (a) Spatial distribution of meteorological stations across China, with brownish-yellow dots indicating station locations; **(b)** latitudinal and longitudinal distributions of the stations; and **(c)** elevation across China.

2.2 Satellite products

As shown in Figure 2, five satellite-based remote sensing products were incorporated in this study, including two precipitation products (IMERG and SM2RAIN-ASCAT), two MODIS land surface temperature (LST) products, and one Advanced Very High Resolution Radiometer (AVHRR) normalized difference vegetation index (NDVI) product. The Integrated Multi-satellite Retrievals for GPM (IMERG) is the Level-3 precipitation product developed under the Global Precipitation Measurement (GPM) mission by the National Aeronautics and Space Administration (NASA) (Huffman et al., 2020). This study employed the IMERG Final Run Version 07B product, which provides quasi-global precipitation estimates at a spatial resolution of 0.1° from June 2000 to 2024 over the latitude band of 60° N–60° S. The dataset was obtained from the NASA Goddard Earth Sciences Data and Information Services Center (GES DISC; https://disc.gsfc.nasa.gov/).The SM2RAIN-ASCAT precipitation product is generated using a soil-moisture-based rainfall retrieval algorithm (Brocca et al., 2019). It provides daily precipitation

https://doi.org/10.5194/essd-2026-704
Preprint. Discussion started: 16 November 2026
© Author(s) 2026. CC BY 4.0 License.


estimates at a spatial resolution of 0.1° over the global land surface for the period 2007–2022. The dataset is publicly available through Zenodo (https://zenodo.org/record/3405563).

Land surface temperature data were derived from the MOD11A1 and MYD11A1 products acquired by the MODIS sensors onboard the Terra and Aqua satellites, respectively. These products provide daily daytime and nighttime LST observations at a spatial resolution of 1 km from 2000 onwards (Wan et al., 2021) and were downloaded from the NASA Level-1 and Atmosphere Archive and Distribution System (LAADS; https://ladsweb.modaps.eosdis.nasa.gov/). In this study, the mean of the daytime and nighttime LST observations was used as a surrogate for mean air temperature, while the daytime and nighttime observations were adopted as proxies for daily maximum and minimum air temperature, respectively.

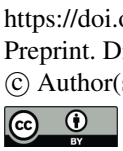
Vegetation information was represented using the normalized difference vegetation index (NDVI) derived from the NOAA Advanced Very High Resolution Radiometer (AVHRR). The AVHRR NDVI product provides observations at a spatial resolution of 0.01° spanning the period from 1981 to 2024 and was obtained from the NOAA National Centers for Environmental Information (NCEI; https://www.ncei.noaa.gov/).

It should be noted that each satellite product was incorporated only within its actual observation period, and the combination of input variables was dynamically adjusted according to data availability. No temporal extrapolation or gap filling was performed for years without satellite observations. Instead, the long-term ERA5-Land reanalysis and other continuously available datasets served as the primary input sources during periods lacking satellite observations, thereby ensuring the temporal continuity and internal consistency of the ChinaMet dataset over the entire period from 1980 to 2024.

2.3 Reanalysis data

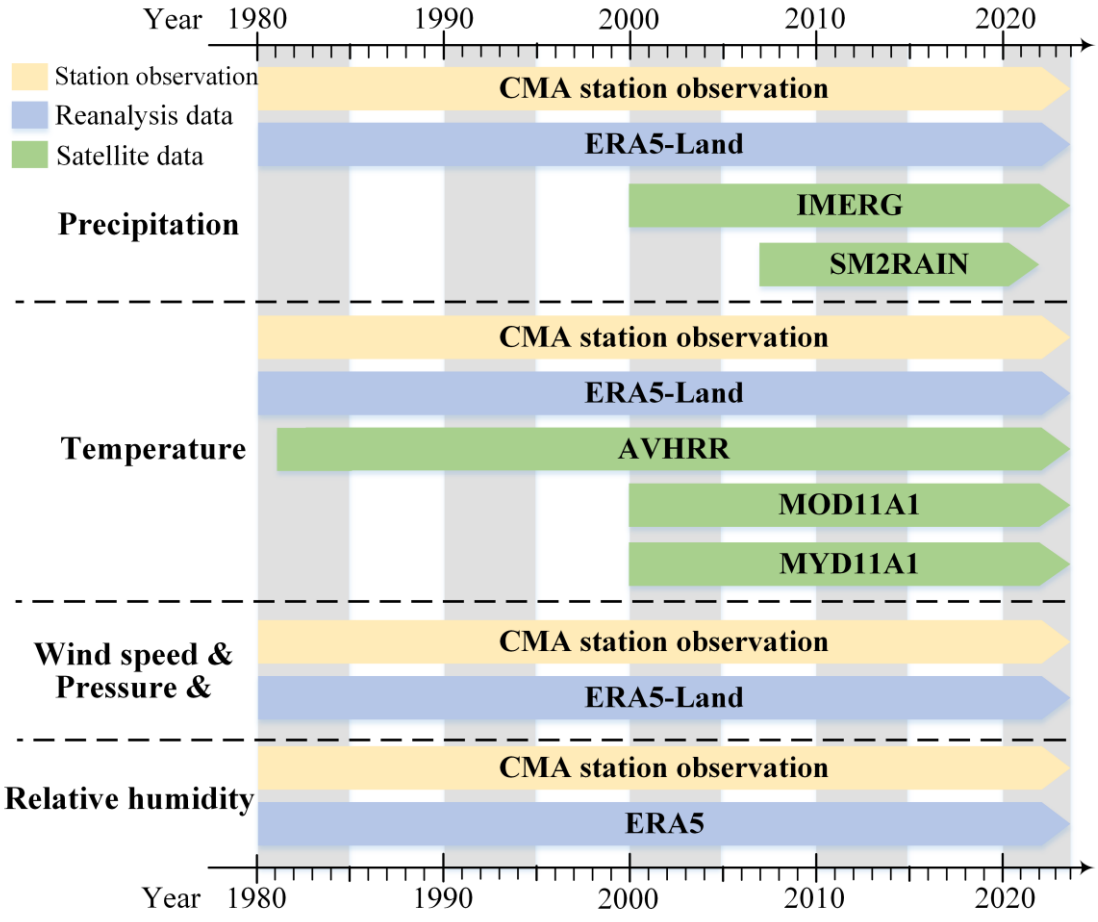
This study employed the fifth-generation ECMWF atmospheric reanalysis (ERA5) and the ERA5-Land land reanalysis datasets produced by the European Centre for Medium-Range Weather Forecasts (ECMWF). Owing to their long temporal coverage, spatiotemporal continuity, and comprehensive set of meteorological variables, these two datasets provide consistent background fields throughout the entire ChinaMet study period (1980–2024) and serve as the foundation for long-term meteorological reconstruction. ERA5 provides hourly atmospheric variables at a spatial resolution of 0.25°, whereas ERA5-Land provides hourly land-surface variables at a finer spatial resolution of 0.1°. While ERA5 covers both the global land surface and oceans, ERA5-Land focuses exclusively on terrestrial surfaces (Muñoz-Sabater et al., 2021). In this study, hourly relative humidity was obtained from ERA5, whereas hourly precipitation, air temperature, wind speed, and surface pressure were extracted from ERA5-Land. All hourly variables were aggregated into daily values over the UTC 00:00–24:00 period to ensure consistency with the temporal definition of the station observations. Both datasets were obtained from the ECMWF Climate Data Store (CDS; https://cds.climate.copernicus.eu/). Because ERA5 and ERA5-Land provide continuous and complete coverage from 1980 to 2024, they were used as the primary predictor datasets throughout the entire reconstruction

https://doi.org/10.5194/essd-2026-704
Preprint. Discussion started: 16 November 2026
© Author(s) 2026. CC BY 4.0 License.



Open Access Earth System Science Data Discussions

period. This provides a temporally consistent baseline for ChinaMet and ensures stable long-term reconstruction despite differences in the temporal availability of individual satellite products.



175 **Figure 2. The data used for ChinaMet**

2.4 Auxiliary data

Digital elevation model (DEM) data were obtained from the Advanced Spaceborne Thermal Emission and Reflection Radiometer Global Digital Elevation Model (ASTER GDEM). The original dataset has a spatial resolution of 30 m and was
180 resampled to 1 km and 10 km to serve as auxiliary predictor variables representing topographic heterogeneity. The dataset is publicly available at https://asterweb.jpl.nasa.gov/gdem.asp. In addition, precipitation statistics were collected from the China Water Resources Bulletin and the Water Resources Bulletins published by provincial-level administrative regions (including provinces, autonomous regions, and municipalities). These records include annual precipitation for 357 prefecture-level cities

https://doi.org/10.5194/essd-2026-704
Preprint. Discussion started: 16 November 2026
© Author(s) 2026. CC BY 4.0 License.

Open Access Earth System Science Data Discussions

during 2011–2020, as well as national annual precipitation statistics covering the period from 1980 to 2024. The water resources bulletins are primarily based on observations from the national meteorological and hydrological station networks and are compiled through statistical analysis and spatial interpolation, providing highly reliable precipitation statistics. In this study, these data were used exclusively as independent reference datasets to evaluate the consistency of ChinaMet precipitation estimates and their long-term variability at both the prefecture and national scales. They were not used for model training.

3 Methodology

The overall workflow of this study is illustrated in Figure 3 and consists of three main components: input data, dataset production, and product evaluation. The input data for ChinaMet include satellite remote sensing products, reanalysis datasets, ground-based meteorological observations, and auxiliary data, as described in Section 2. To identify the optimal production strategy, a station-based stratified hold-out validation was conducted to compare the accuracy and computational efficiency of different approaches. Specifically, 30 % of the observation stations within each of the eight geographical regions of China were randomly selected as independent validation stations, while the remaining stations were used for model development. Based on the overall validation performance and computational efficiency, the Merging–Downscaling (MD) strategy was selected as the final production framework for ChinaMet. Under this strategy, a 0.1° meteorological dataset is first generated using the Random Forest (RF) algorithm and subsequently downscaled to 0.01° using the Climatically Aided Interpolation (CAI) method. Details of the production strategy are provided in Section 3.1. The final ChinaMet dataset was comprehensively evaluated in terms of spatial consistency, independent validation against the China Water Resources Bulletin, and uncertainty analysis.

https://doi.org/10.5194/essd-2026-704
Preprint. Discussion started: 16 November 2026
© Author(s) 2026. CC BY 4.0 License.

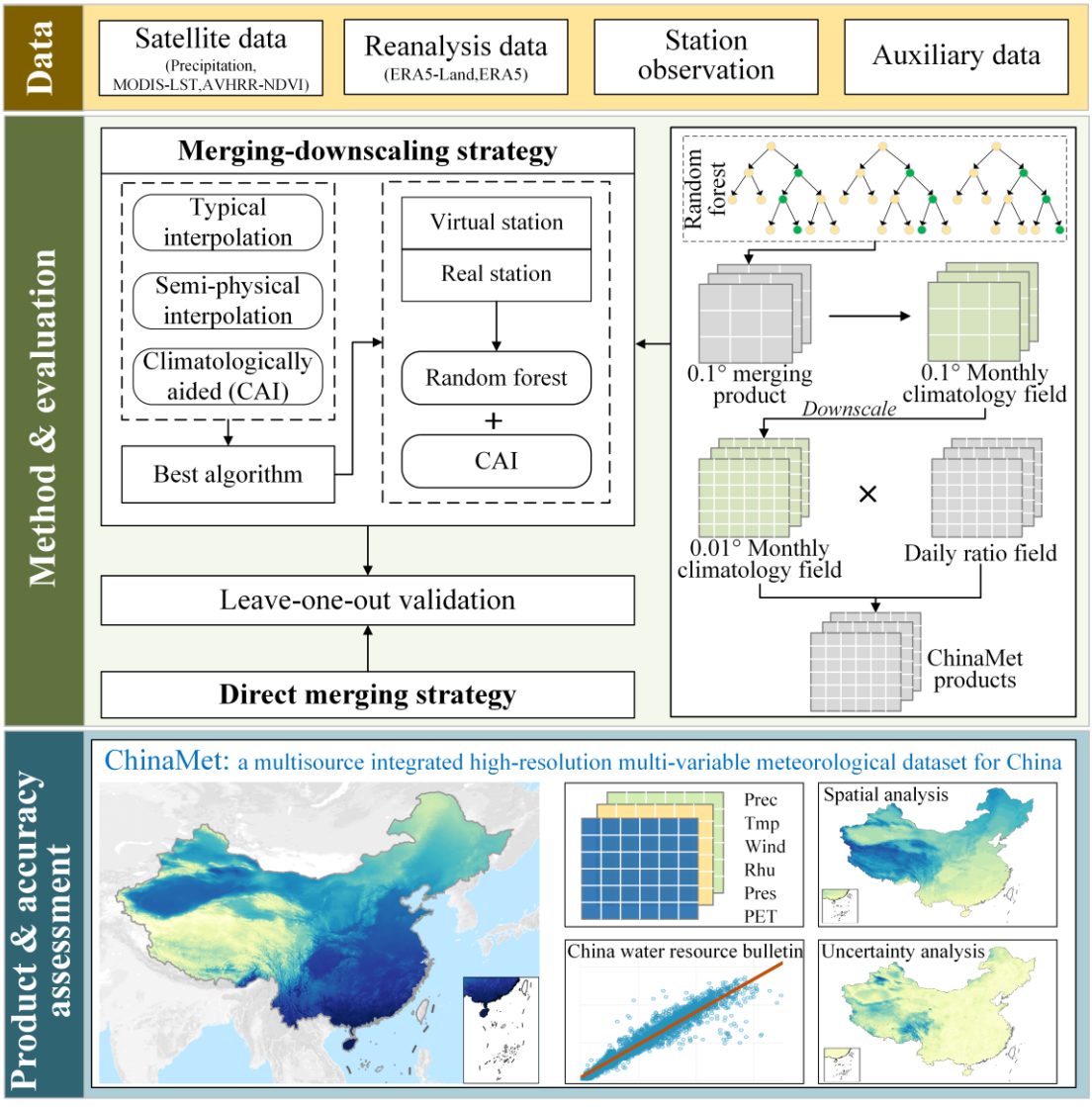


Figure 3. Workflow of this study

3.1 Merging-downscaling strategy

As shown in Figure 3, ChinaMet was developed using the merging–downscaling (MD) strategy, whereas the direct-merging (DM) strategy was implemented as a benchmark to evaluate the computational efficiency of the MD strategy and the associated loss of accuracy. Under the DM strategy, random forest (RF) is applied directly to generate ChinaMet at a spatial resolution of 0.01°. Producing a single daily field requires approximately 8 h because the 0.01° grid over China contains more than nine million grid cells, resulting in a substantial computational burden for both spatial interpolation and batch RF-based data

https://doi.org/10.5194/essd-2026-704
Preprint. Discussion started: 16 November 2026
© Author(s) 2026. CC BY 4.0 License.



merging. The MD strategy was therefore adopted primarily because it substantially improves computational efficiency while introducing only a marginal loss of accuracy. A virtual-station approach was also incorporated into the dataset-development framework to improve meteorological estimates in regions with sparse or absent ground observations (Thiemig et al., 2022). Candidate virtual stations were restricted to observation-sparse 0.75° grid cells, with an additional proximity criterion used to avoid introducing virtual observations near existing ground stations. The corresponding reanalysis estimates were assigned as virtual-station values, using ERA5-Land for precipitation, air temperature, wind speed, and surface pressure and ERA5 for relative humidity. The effects and associated uncertainties of the virtual-station approach are further discussed in Section 5.1. The MD and DM strategies are described separately below.

The DM strategy generates the meteorological products using a machine-learning algorithm, namely RF. First, the optimal method was selected from conventional interpolation, semi-physical interpolation, and climatologically aided interpolation (CAI) through five-fold cross-validation at the meteorological stations. The corresponding optimal geographical auxiliary predictor, NE, was then derived and incorporated into the RF model to improve its ability to represent nonlinear relationships (Hu and Zhang, 2024). RF is an ensemble-learning method based on regression and classification trees and has been widely applied to multi-source data merging. In this study, RF was implemented using the TreeBagger function in MATLAB, which supports both decision-tree construction and prediction. Following repeated sensitivity experiments, the number of trees (Ntree) and the minimum number of observations per terminal leaf (MinObs) were set to 300 and 20, respectively. The satellite and reanalysis datasets used for the different meteorological variables are summarized in Figure 2. For precipitation estimation, an RF classifier was first used to distinguish dry days, defined as days without precipitation, from wet days, defined as days with precipitation. An RF regression model was subsequently used to estimate precipitation amounts on wet days. The procedure is expressed in Eq. 1.

$$P_p = \begin{cases} \hat{y}(x)_{regression}, wet \\ 0 \qquad\qquad\quad , \text{dry} \end{cases} \tag{1}$$

Where $\hat{y}(x)_{regression}$ denotes the value predicted by the random forest regression model, and x represents the predictor variables used for precipitation estimation. These predictors include geographical covariates (longitude, latitude, elevation, and regional ID), spatial-autocorrelation variables (NE and POP), satellite observations (IMERG and SM2RAIN), and ERA5-Land reanalysis data. The term ε denotes the weighted mean bias derived from neighboring stations. Further details on the input variables are provided in our previous studies (Zhang et al., 2021; Hu and Zhang, 2024).

The merging–downscaling strategy combines RF-based data merging with climatologically aided interpolation (CAI). First, the direct-merging approach is used to generate an initial product at a spatial resolution of 0.1°, from which monthly climatological fields are constructed. These climatological fields are then downscaled to produce monthly data at 0.01° resolution (Jiang et al., 2023b). For precipitation, CAI was implemented using ratio fields, whereas climatological anomaly fields were used for air temperature, relative humidity, wind speed, and surface pressure. Climatologically aided interpolation is an interpolation method that integrates long-term climatological information with short-term station observations to improve

https://doi.org/10.5194/essd-2026-704
Preprint. Discussion started: 16 November 2026
© Author(s) 2026. CC BY 4.0 License.



Open Access Earth System Science Data Discussions

estimation accuracy. Its principal advantage is that it incorporates not only direct observations from meteorological stations but also the long-term climatic background. CAI has therefore been widely used to generate high-quality climate datasets (Willmott and Robeson, 1995). Specifically, CAI combines historical climatological fields with station observations to derive either ratio or anomaly fields. The final estimates are then obtained by multiplying the ratio field by, or adding the anomaly field to, the corresponding climatological background field. For precipitation, CAI is implemented using ratio fields, as expressed in Eq. 2 and Eq. 3:

$$R_i = \frac{P_i}{P_{ce}^{Known}} \tag{2}$$

$$P_{\mathrm{p}} = P_{ce}^{Pred} \times \frac{\sum_{i=1}^{n} W_i R_i}{\sum_{i=1}^{n} W_i} \tag{3}$$

Where R_i denotes the ratio calculated for the i^{th} neighboring station, P_i is the precipitation value at the ith neighboring station, and P_{ce} represents the ChinaMet climatological mean monthly accumulated precipitation for 1980–2020. The superscripts $Pred$ and $Known$ denote the prediction location and the neighboring station with known observations, respectively. W_i is the weight assigned to the ith neighboring station using the DAYMET weighting scheme (Thornton et al., 1997; Stahl et al., 2006), as defined in Eq. 4.

$$w_i = \begin{cases} exp\left[-\left(\frac{d_i}{R_p}\right)^2 \alpha\right], d_i \le R_p \\ 0 \qquad\qquad\qquad\quad , d_i > R_p \end{cases} \tag{4}$$

Where R_p denotes the cutoff radius and α is the shape parameter. Notably, the cutoff radius R_p for each prediction grid cell is adaptively determined through an iterative procedure based on the local station density. A smaller R is used in areas with dense station coverage, whereas a larger R is adopted in regions where stations are sparse.

For the other meteorological variables, including air temperature, relative humidity, wind speed, and surface pressure, CAI primarily performs interpolation using climatological anomaly fields (Willmott and Robeson, 1995). The corresponding calculations are expressed in Eq. 5 and Eq. 6:

$$D_i = P_i - P_{ce}^{Known} \tag{5}$$

$$P_p = P_{ce}^{pred} + \frac{\sum_{i=1}^{n} W_i D_i}{\sum_{i=1}^{n} W_i} \tag{6}$$

where D_i denotes the anomaly calculated at the i^{th} neighboring station, and P_{ce} represents the 1980–2020 monthly climatology of the corresponding ERA5-Land variable. All other symbols have the same definitions as those in Eq. 2 and Eq. 3.

https://doi.org/10.5194/essd-2026-704
Preprint. Discussion started: 16 November 2026
© Author(s) 2026. CC BY 4.0 License.



3.2 Method evaluation

The performance of the two production strategies was evaluated using a station-based stratified hold-out validation. After acquiring and processing all input datasets, the Random Forest (RF) algorithm and five spatial interpolation methods, namely inverse distance weighting (IDW), Kriging, geographical difference analysis interpolation system (GIDS), DAYMET, and climatically aided interpolation (CAI), were implemented in the MATLAB environment. A total of more than 2,300 meteorological observation stations during the period 2015–2020 were used for the evaluation. The stations were stratified according to the eight geographical regions of China, and within each region, 30 % of the observation stations were randomly selected as independent validation stations, while the remaining 70 % were used for model training (Hu and Zhang, 2024). This stratified sampling strategy ensures a spatially balanced distribution of the training and validation datasets across the study area. Virtual stations were used exclusively for model construction and were not included in the validation set or in the calculation of the final evaluation metrics. Both the Merging–Downscaling (MD) and Direct–Merging (DM) strategies were evaluated using the same training and validation stations to ensure a fair and directly comparable assessment of their performance.

Several statistical metrics were used to evaluate the performance of the interpolation and data-merging methods. The Kling–Gupta efficiency (KGE) was adopted as an integrated performance metric comprising the correlation coefficient (CC), bias ratio (β), and variability ratio (γ). KGE jointly accounts for correlation, systematic bias, and relative variability when evaluating agreement between predictions and station observations (Gupta et al., 2009). We also used the coefficient of determination (R^2) and root-mean-square error (RMSE), which quantify the degree of agreement and the magnitude of errors between predicted and observed values. Table 1 presents the equations and optimal values of these metrics, where P and O denote the predicted and observed station values, respectively; μ and σ represent the mean and standard deviation; i denotes the time step; and n is the total number of time steps. The theoretical ranges of KGE, CC, R^2, and RMSE are $(-\infty,1]$, $[-1,1]$, $[0,1]$, and $[0,\infty)$, respectively. KGE and its components indicate better predictive performance as their values approach 1. Similarly, an R^2 value closer to 1 indicates that the model explains a larger proportion of the observed variability, whereas a lower RMSE indicates greater predictive accuracy.

Table 1 The evaluation metrics used in this study

Metrics	Formula	Perfect value
KGE	$KGE = 1 - \sqrt{(1-CC)^2 + (1-\text{ Beta })^2 + \left(1-\text{ Gama }^2\right)^2}$	1
CC	$CC = \frac{\Sigma_{i=1}^{n}\left(P_i^{pre} - P_{mean}^{pre}\right)(O_i - O_{mean})}{\sqrt{\Sigma_{i=1}^{n}\left(P_i^{pre} - P_{mean}^{pre}\right)^2}\sqrt{\Sigma_{i=1}^{n}(O_i - O_{mean})^2}}$	1

https://doi.org/10.5194/essd-2026-704
Preprint. Discussion started: 16 November 2026
© Author(s) 2026. CC BY 4.0 License.



Beta	$Beta = \frac{\mu_{pre}}{\mu_O}$	1
Gama	$Gama = \frac{\sigma_{pre}/\mu_{pre}}{\sigma_{O/\mu_o}}$	1
R^2	$R^2 = 1 - \frac{\sum_{i=1}^{n}\left(P_i^{\text{pre}} - O_i\right)^2}{\sum_{i=1}^{n}\left(P_i^{\text{pre}} - O_{\text{mean}}\right)^2}$	1
RMSE	$RMSE = \sqrt{\frac{1}{n}\sum_{i=1}^{n}\left(P_i^{\text{pre}} - O_i\right)^2}$	0

3.3 Product development and accuracy assessment

3.3.1 Product development

With the exception of potential evapotranspiration (PET), the primary data sources used to generate the other ChinaMet meteorological variables are shown in Figure 2. All these variables were produced using the merging-downscaling strategy. First, the random forest algorithm was used to generate products at a spatial resolution of 0.1° for 1980–2024. Monthly ratio climatology and monthly anomaly climatology were then calculated from the initial products and used in the CAI downscaling procedure to generate the corresponding 0.01° products for 1980–2024.

Potential evapotranspiration was estimated using two commonly applied methods, namely the Penman-Monteith and Hargreaves methods. The Penman-Monteith method is recommended by the Food and Agriculture Organization of the United Nations (FAO) for estimating potential evapotranspiration. Because it accounts for the principal meteorological controls on evapotranspiration, the Penman-Monteith model has a relatively strong physical basis. PET was calculated using the Penman-Monteith equation as follows:

$$PET = \frac{0.408\Delta(R_n - G) + \gamma\frac{900}{T+273}u_2(e_s - e_a)}{\Delta + \gamma(1 + 0.34u_2)} \quad (7)$$

where PET denotes potential evapotranspiration (mm/day); Δ is the slope of the saturation vapor pressure curve (kPa/°C); Rn is the net radiation (MJ/m^2 day); G is the soil heat flux (MJ/m^2 day); γ is the psychrometric constant (kPa °C^{-1}); T is the mean air temperature at 2 m above the ground (°C); u_2 is the mean wind speed at 2 m above the ground (m s^{-1}); and e_s and e_a are the saturation vapor pressure and actual vapor pressure at 2 m above the ground, respectively (kPa).

The variables required for potential evapotranspiration (PET) estimation were derived from the ChinaMet meteorological variables and auxiliary datasets. Net radiation (R_n) was calculated as the difference between net shortwave

https://doi.org/10.5194/essd-2026-704
Preprint. Discussion started: 16 November 2026
© Author(s) 2026. CC BY 4.0 License.



radiation (R_{ns}) and net longwave radiation (R_{nl}). Specifically, R_{ns} was estimated from the daily maximum and minimum air temperatures, latitude, and day of the year, whereas R_{nl} was estimated using the daily maximum and minimum air temperatures, actual vapor pressure, and clear-sky radiation conditions. The 10 m wind speed provided by ChinaMet was converted to the standard 2 m height using the FAO-56 logarithmic wind profile relationship $u_2 = u_z \frac{4.87}{ln(67.8z-5.42)}$. Saturation vapor pressure was calculated from the daily maximum and minimum air temperatures, whereas actual vapor pressure was derived from the dew-point temperature estimated using the daily mean relative humidity and air temperature. The slope of the saturation vapor pressure curve was calculated from the daily mean air temperature. These variables were subsequently used in the FAO-56 Penman–Monteith equation to estimate daily potential evapotranspiration (PET).

In contrast, the empirical Hargreaves method estimates potential evapotranspiration using only daily mean air temperature and the diurnal temperature range (Ding and Peng, 2021). The equation is expressed as follows:

$$PET = 0.0023(T_{mean} + 17.8)(T_{\max} - T_{min})^{0.5} Ra \quad (8)$$

where T_{mean}, T_{max} and T_{min} denote the daily mean, maximum, and minimum air temperatures, respectively, and R represents the daily extraterrestrial radiation, which can be calculated from latitude and the day of year.

As shown in Table 2, ChinaMet provides eight meteorological variables: precipitation (pre), 2 m mean air temperature (tmpmean), 2 m maximum air temperature (tmpmax), 2 m minimum air temperature (tmpmin), 10 m wind speed (wind), relative humidity (rhu), surface pressure (pres), and potential evapotranspiration (pet). The dataset covers the period from 1980 to 2024 and is available at spatial resolutions of 0.1° and 0.01°, with the latter corresponding to approximately 1 km at mid-latitudes. Annual, monthly, and daily temporal resolutions are provided. Each file follows the naming convention ChinaMet_%S_%V_%T.nc, where %S denotes the spatial resolution, %V represents the variable name, and %T indicates the temporal resolution.

Table 2 Overview of the ChinaMet product

Variable	Spatiotemporal resolution	NetCDF field name
Precipitation (mm)	Daily/monthly/yearly 1980-2024 0.1°/0.01°	prec
2-m daily mean air temperature (℃)	Daily/monthly/yearly 1980-2024 0.1°/0.01	tmpmean
2-m daily maximum air temperature (℃)	Daily/monthly/yearly 1980-2024 0.1°/0.01	tmpmax

https://doi.org/10.5194/essd-2026-704
Preprint. Discussion started: 16 November 2026
© Author(s) 2026. CC BY 4.0 License.



2-m daily minimum air temperature (℃)	Daily/monthly/yearly 1980-2024 0.1°/0.01	tmpmin
Surface pressure (hPa)	Daily/monthly/yearly 1980-2024 0.1°/0.01	pres
2-m relative humidity (%)	Daily/monthly/yearly 1980-2024 0.1°/0.01	rhu
10-m wind speed (m/s)	Daily/monthly/yearly 1980-2024 0.1°/0.01	wind
Potential evapotranspiration (mm)	Daily/monthly/yearly 1980-2024 0.1°/0.01	petHG petPM

3.3.2 Product evaluation

To systematically evaluate the accuracy and practical applicability of the multi-variable ChinaMet dataset, we conducted assessments from four perspectives: comparison of spatial patterns, pointwise agreement analysis using scatterplots and density plots, validation against precipitation statistics from water resources bulletins, and uncertainty assessment. As shown in Table 3, the multi-variable meteorological datasets selected for comparison included CDMet, CMFD, ERA5-Land, and MSWX. CHM is a precipitation-only product, whereas CDAT provides air temperature only. We compared the spatial patterns of ChinaMet with those of five other products over the common period of 2000–2018, focusing on whether the spatial characteristics of ChinaMet were consistent with those of widely used products. Their agreement was further examined using scatterplots and density plots. In addition, the TCH method was applied to compare the monthly TCH-derived absolute uncertainties of ChinaMet and the other products during 2000–2018. For precipitation, we also compared the spatial patterns of the six products over the Qinghai-Tibet Plateau (QTP). Precipitation statistics from water resources bulletins were used as an independent reference to evaluate the 2011–2020 mean annual precipitation estimates and relative trends of ChinaMet and five other precipitation products at the prefecture-level administrative scale. The national annual precipitation series reported in the water resources bulletins for 1997–2022 was also used for trend comparison.

https://doi.org/10.5194/essd-2026-704
Preprint. Discussion started: 16 November 2026
© Author(s) 2026. CC BY 4.0 License.



350 Table 3 Datasets used to evaluate ChinaMet and their spatiotemporal resolutions

Variable	Product name	Spatiotemporal resolution
Precipitation (mm)	ChinaMet	2000-2018 0.01°
	CDMet	2000-2018 0.1°
	CMFD	2000-2018 0.1°
	CHM	2000-2018 0.1°
	ERA5-Land	2000-2018 0.1°
	MSWX	2000-2018 0.1°
2-m air temperature (℃)	ChinaMet	2000-2018 0.1°
	CDMet	2000-2018 0.1°
	CMFD	2000-2018 0.1°
	CDAT	2000-2018 0.1°
	ERA5-Land	2000-2018 0.1°
	MSWX	2000-2018 0.1°
Surface pressure (hPa) & 2-m relative humidity (%) & 10-m wind speed (m/s)	ChinaMet	2000-2018 0.1°
	CDMet	2000-2018 0.1°
	CMFD	2000-2018 0.1°
	ERA5-Land	2000-2018 0.1°
	MSWX	2000-2018 0.1°
Potential evapotranspiration (mm)	ChinaMet-petPM	2000-2018 0.01°
	ChinaMet-petHG	2000-2018 0.01°

https://doi.org/10.5194/essd-2026-704
Preprint. Discussion started: 16 November 2026
© Author(s) 2026. CC BY 4.0 License.



PET-Peng	2000-2018 0.1°
GLEAM	2000-2018 0.1°
CRU-TS	2000-2018 0.1°
ERA5	2000-2018 0.1°

3.3.3 Uncertainty analysis

To quantitatively assess the uncertainties of ChinaMet and comparable products, this study employed the generalized form of the Three-Cornered Hat (TCH) method. The TCH method estimates the error variance of each product without requiring a true reference value and can be applied when more than three products are evaluated (Ferreira et al., 2016; Xu et al., 2019; Sjoberg et al., 2021). The TCH method is formulated as follows:

$$X_i = X_t + \varepsilon_i,\ i = 1,2,3,\dots,N \tag{9}$$

where the time series of the i^{th} product is denoted by X_i, with $i = 1,2,\dots,N$, and N representing the total number of products. Each product time series X_i consists of the unknown true value X_t and an associated error term ε_i. Because the true signal X_t is unknown, the TCH method eliminates it by differencing the individual products. In this study, the N^{th} product was selected as the computational reference, and the difference between each of the remaining products and the reference product was calculated as:

$$Y_i = X_i - X_N = \varepsilon_i - \varepsilon_N,\ i = 1,2,\dots,N-1 \tag{10}$$

The selection of X_N is used only to construct the difference series and does not imply that this product represents the true value. All difference series were assembled into the matrix Y. The covariance matrix of the difference series, S, and the error covariance matrix of the original products R were defined as:

$$S = cov(Y), R = cov(\varepsilon) \tag{11}$$

where the diagonal elements R_{ii} represent the error variances of the individual products, whereas the off-diagonal elements describe the error covariances between products. The two covariance matrices are related by:

$$S = J \cdot R \cdot J^{-1} \tag{12}$$

where J denotes the differencing matrix. The complete error covariance matrix R cannot be obtained directly from S. Following the generalized TCH framework described by Ferreira et al., 2016, the elements in the last column of R, R_{1N}, $R_{2N}, \dots, R_{NN}$ were first estimated through constrained nonlinear optimization. In this study, the optimization was implemented using the MATLAB fmincon function. Once these terms were obtained, the remaining elements of R were reconstructed as

https://doi.org/10.5194/essd-2026-704
Preprint. Discussion started: 16 November 2026
© Author(s) 2026. CC BY 4.0 License.



$$R_{ij} = S_{ij} - R_{NN} + R_{iN} + R_{jN}, i, j = 1,2, \dots, N-1 \quad (13)$$

Accordingly, setting $i = j$ gives the error variance of each non-reference product. The absolute uncertainty was then calculated as the standard deviation of the estimated error:

$$R_{ii} = S_{ii} - R_{NN} + 2R_{iN}, \ \sigma_i = \sqrt{R_{ii}} \quad (14)$$

where σ_i denotes the absolute uncertainty of the i^{th} product. For the computational reference product, its error variance is directly given by R_{NN}, and its absolute uncertainty is therefore $\sqrt{R_{NN}}$. The absolute uncertainty retains the physical unit of the corresponding variable; thus, it is expressed in mm month^{-1} for monthly precipitation and in °C for monthly mean air temperature.

The relative uncertainty was additionally calculated by normalizing the absolute uncertainty by the mean absolute magnitude of the corresponding product:

$$RU_i = \frac{\sqrt{\sigma_i}}{|x_i|} \times 100\% \quad (15)$$

where $\overline{|x_i|}$ denotes the mean absolute value of product i^{th} product over the analysis period. The relative uncertainty is dimensionless and is expressed as a percentage (%). The TCH calculations were performed independently at each grid cell using monthly data during 2000–2018. Both absolute and relative uncertainties were calculated for each product. The spatial uncertainty distributions and inter-product comparisons presented in Figures 12 and 13 are based on the absolute uncertainty σ_i.

4 Results

4.1 Evaluation of the merging-downscaling strategy

As shown in Figure 4, the station observations from 2015 to 2020 were used to compare the estimation accuracy and computational efficiency of the Merging–Downscaling (MD) and Direct–Merging (DM) strategies using the station-based stratified hold-out validation described in Sect. 3.2. Specifically, 30 % of the observation stations within each of the eight geographical regions of China were randomly selected as independent validation stations. The computational efficiency of both strategies was evaluated on two hardware platforms, an Intel(R) Core(TM) i5-10400 6-core processor and an Intel(R) Core(TM) i9-13900K 24-core processor. The total computational time required to generate all ChinaMet meteorological variables for the period 1980–2024 was also recorded (Figure 4d). The MD and DM strategies exhibited comparable predictive performance for most meteorological variables, with only marginal differences in overall accuracy. The Kling–Gupta efficiency (KGE) values were nearly identical, with differences of less than 0.1 between the two strategies (Figure 4a). Similarly, the coefficient of determination (R^2) and root mean square error (RMSE) showed only minor differences, with the absolute differences in both metrics remaining below 0.05. In contrast, the MD strategy substantially improved computational

https://doi.org/10.5194/essd-2026-704
Preprint. Discussion started: 16 November 2026
© Author(s) 2026. CC BY 4.0 License.



efficiency. Compared with the DM strategy, the total processing time required to generate the complete ChinaMet dataset decreased from 355 days to 42 days, corresponding to an approximately 89 % reduction in computational time. Overall, the MD strategy achieved predictive accuracy comparable to that of the DM strategy while substantially reducing computational cost. Therefore, the MD strategy was selected as the final production framework for ChinaMet, providing a more efficient solution for producing large-scale, high-resolution, multi-variable meteorological datasets.

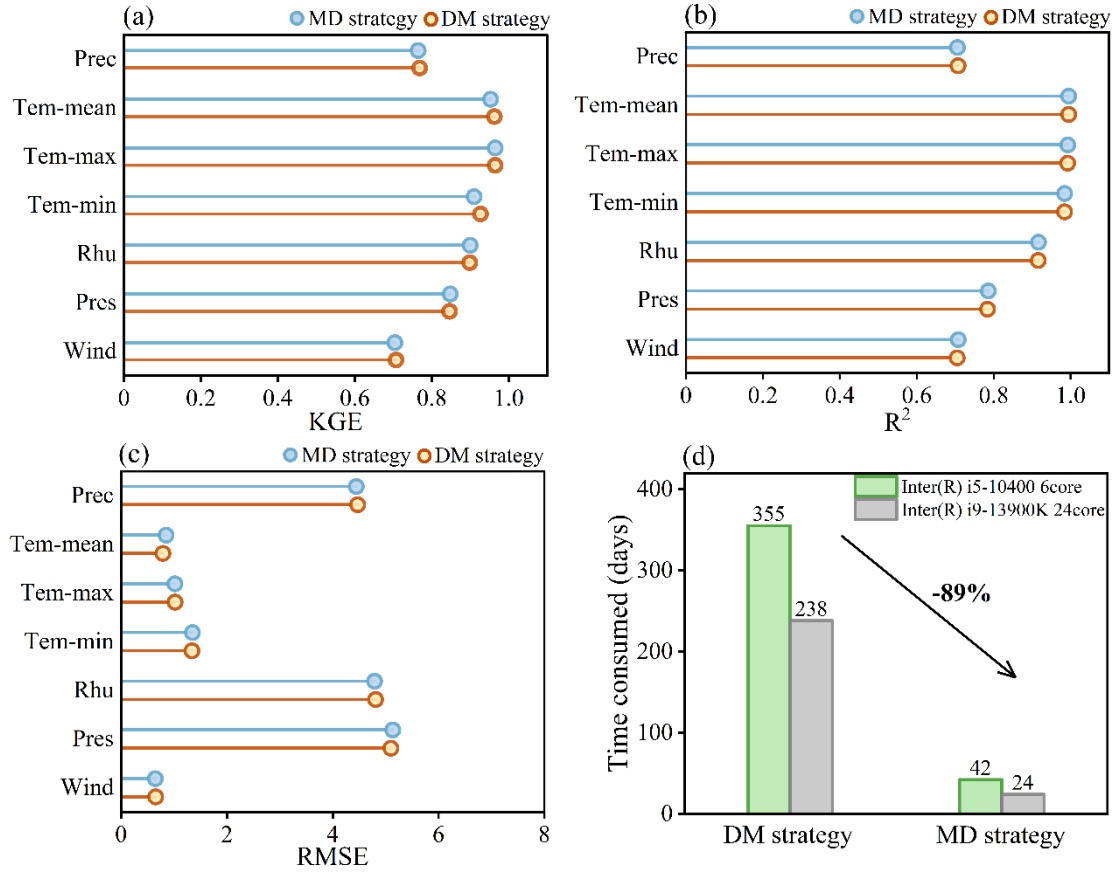


Figure 4. Comparison of the accuracy and computational efficiency of the Merging–Downscaling (MD) and Direct–Merging (DM) strategies.

4.2 Accuracy of ChinaMet

As shown in Figure 5, precipitation statistics from the China Water Resources Bulletin were used as an independent reference to evaluate the external consistency of ChinaMet and five other precipitation products. Annual precipitation from the six datasets was compared with the annual precipitation statistics reported for 357 prefecture-level administrative regions during 2011–2020. It should be noted that the precipitation statistics reported in the China Water Resources Bulletin are primarily

https://doi.org/10.5194/essd-2026-704
Preprint. Discussion started: 16 November 2026
© Author(s) 2026. CC BY 4.0 License.


derived from long-term observations collected by the national meteorological and local hydrological station networks and are compiled through statistical analysis, spatial interpolation, and quality control, providing a reliable independent reference for product evaluation. Among the six precipitation products, ChinaMet achieved the best overall performance, with an R^2 of 0.92, an RMSE of 177 mm yr^{-1}, and a Bias of −26 mm yr^{-1}. CHM and CMFD ranked second, with R^2 values of 0.91 and 0.90, respectively. In contrast, ERA5-Land exhibited a clear positive bias, with an R^2 of 0.81 and a Bias of 126 mm yr^{-1}. Figure 6 further compares the ability of the six precipitation products to reproduce the relative precipitation trends reported in the prefecture-level water resources bulletins. ChinaMet and CHM showed the highest trend detection accuracy, correctly identifying 85 % and 84 % of the observed trends, respectively. CDMet and CMFD performed similarly, with accuracies of 80 % and 79 %, whereas ERA5-Land and MSWX achieved accuracies of only 59 %. Their errors were predominantly concentrated in the first and fourth quadrants, indicating frequent misclassification of trend directions. This is likely attributable to the relatively sparse station observations incorporated into these two datasets over China, limiting their ability to capture precipitation trends at the prefecture scale. As shown in Supplementary Figure S1 and Table 4, the six precipitation products were further compared with the national annual precipitation statistics reported in the China Water Resources Bulletin for the period 1997–2022, using the longest available time series for each dataset. ChinaMet and CMFD showed the closest agreement with the national precipitation statistics and exhibited the lowest Bias values among all products, with Bias values of 15.23 mm yr^{-1} and −15.89 mm yr^{-1}, respectively. Overall, ChinaMet demonstrated the highest consistency with the China Water Resources Bulletin in terms of both annual precipitation estimates and long-term precipitation trends at the prefecture scale, outperforming the other precipitation products evaluated in this study.

https://doi.org/10.5194/essd-2026-704
Preprint. Discussion started: 16 November 2026
© Author(s) 2026. CC BY 4.0 License.

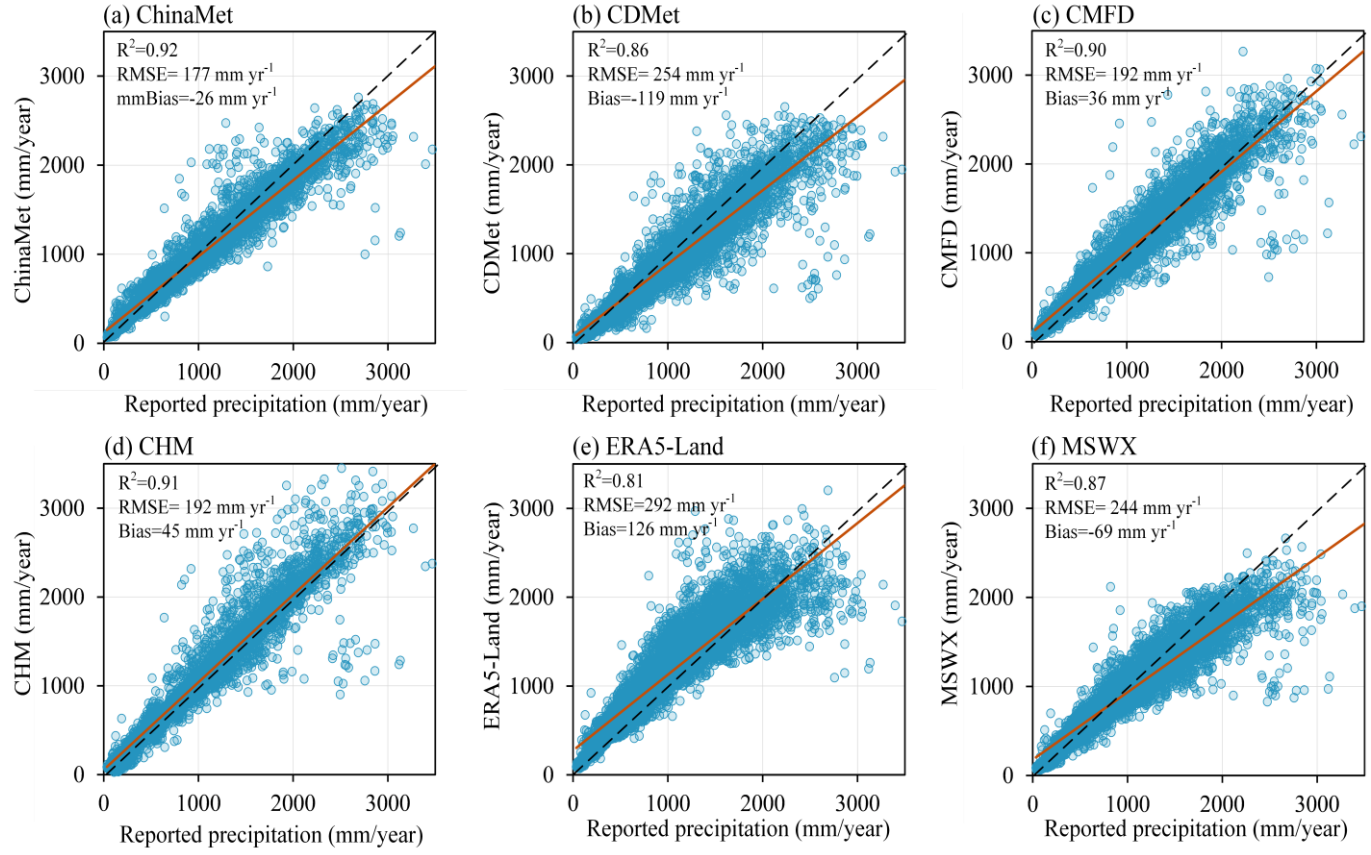


Figure 5. Scatterplots comparing mean annual precipitation from six precipitation products with estimates from municipal water resources bulletins at the prefecture-level administrative-unit scale during 2011–2020.

https://doi.org/10.5194/essd-2026-704
Preprint. Discussion started: 16 November 2026
© Author(s) 2026. CC BY 4.0 License.

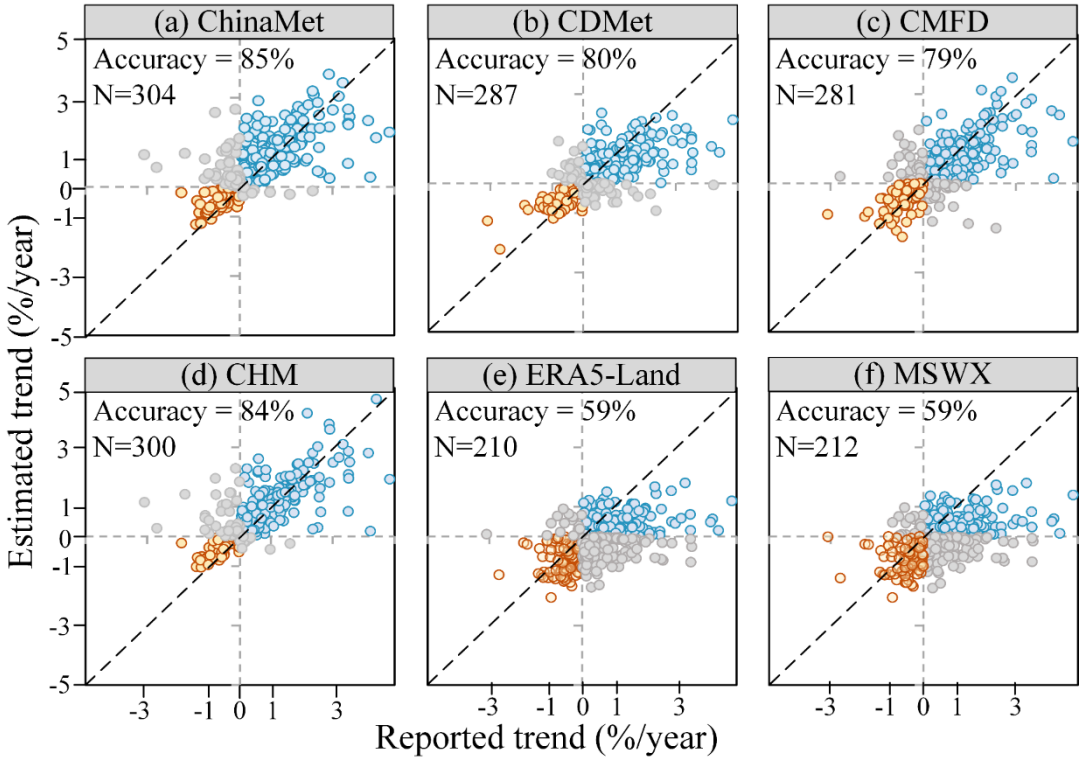


Figure 6. Relative trends in annual precipitation from six precipitation products and municipal water resources bulletins during 2011–2020 (% /yr).

Table 4. Bias and relative bias of precipitation products against the National Water Resources Bulletins during 1997–2022. CMFD and CDMet are available only through 2018 and 2020, respectively.

Product	Bias (mm/year)	Relative bias
ChinaMet (1997-2022)	15.23	0.03
CMFD (1997-2018)	-15.89	-0.02
CDMet (2000-2020)	-119.49	-0.18
CHM (1997-2022)	-28.56	-0.04
E5L (1997-2022)	140.34	0.22
MSWX (1997-2022)	-53.70	-0.08

Figure 7 shows the spatial distribution of mean annual precipitation during 2000–2018 derived from ChinaMet and five other precipitation products, together with the 200, 400, and 800 mm isohyets. The figure also reports the mean annual precipitation at the 30 % hold-out observation stations that were excluded from the development of ChinaMet. Here, M.c denotes the mean

https://doi.org/10.5194/essd-2026-704
Preprint. Discussion started: 16 November 2026
© Author(s) 2026. CC BY 4.0 License.


annual precipitation estimated by each product at the hold-out stations, and M.o denotes the corresponding station observations. ChinaMet reproduces the southeast-to-northwest precipitation gradient across China, with annual precipitation exceeding 2000 mm yr^{-1} in South China and the middle and lower Yangtze River Basin, and less than 400 mm yr^{-1} in northwestern China. The precipitation gradient is spatially continuous and consistent with the observed climate pattern. The 800 mm isohyet extends westward along the Qinling–Huaihe line, the 400 mm isohyet remains continuous across the agro-pastoral ecotone, and the 200 mm isohyet clearly delineates the extremely arid regions of the Tarim Basin. Among the six products, ChinaMet shows the closest spatial agreement with CDMet. The locations of the 800 mm and 400 mm isohyets are nearly identical, and the corresponding M.c values are 900.54 and 891.00 mm yr^{-1}, respectively, which are closest to the observed M.o value of 905.52 mm yr^{-1}. CMFD and CHM reproduce the overall precipitation gradient but show a slight contraction of the 800 mm isohyet over South China and fluctuations of the 400 mm isohyet in northern China. MSWX exhibits a systematic dry bias, with the 800 mm isohyet shifted southward and the 200 mm isohyet shifted eastward. ERA5-Land shows a systematic wet bias, with the 800 and 400 mm isohyets displaced northward. Figure 8 further compares the spatial consistency between ChinaMet and the other precipitation products. Most products show correlation coefficients (CCs) greater than 0.80 with ChinaMet. ERA5-Land has the highest correlation (CC = 0.89), reflecting its use as a source of virtual stations in regions with sparse observations, such as the Tibetan Plateau.

https://doi.org/10.5194/essd-2026-704
Preprint. Discussion started: 16 November 2026
© Author(s) 2026. CC BY 4.0 License.

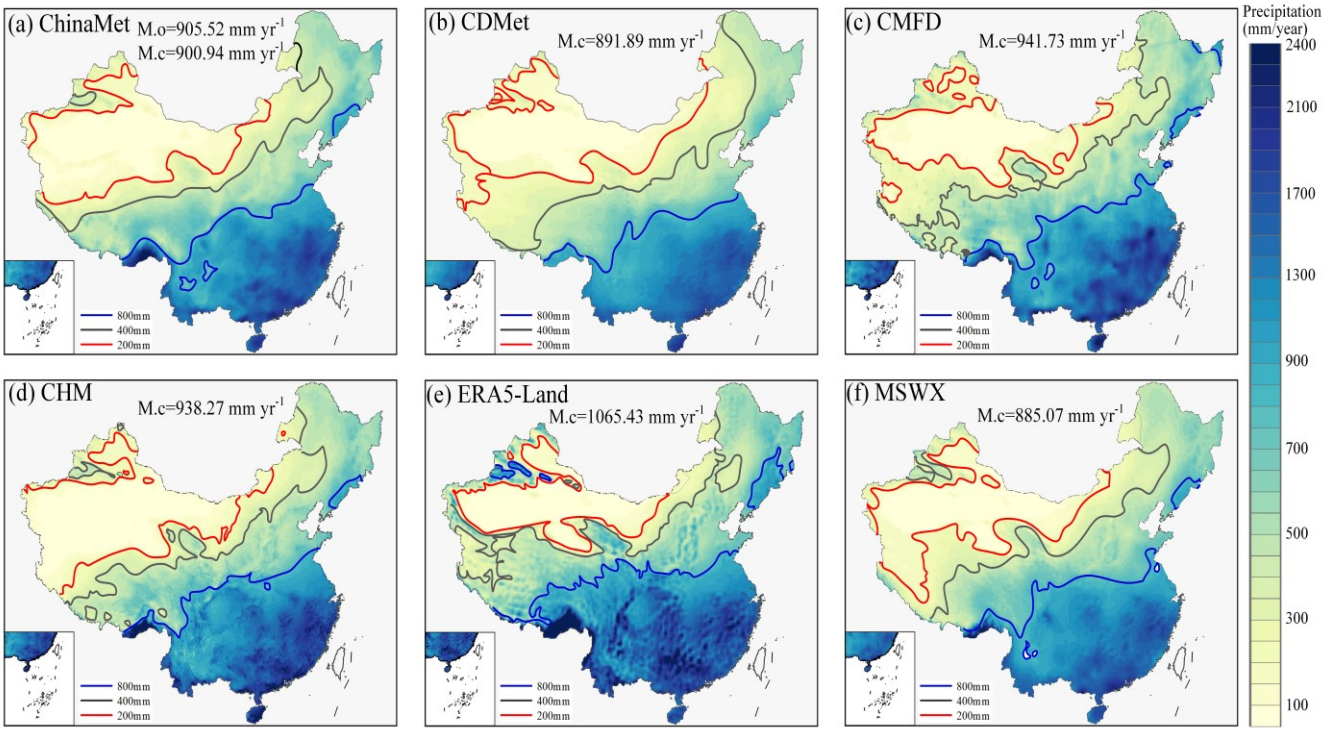


Figure 7. Spatial distributions of multiyear mean annual precipitation from six precipitation products during 2000–2018.

https://doi.org/10.5194/essd-2026-704
Preprint. Discussion started: 16 November 2026
© Author(s) 2026. CC BY 4.0 License.

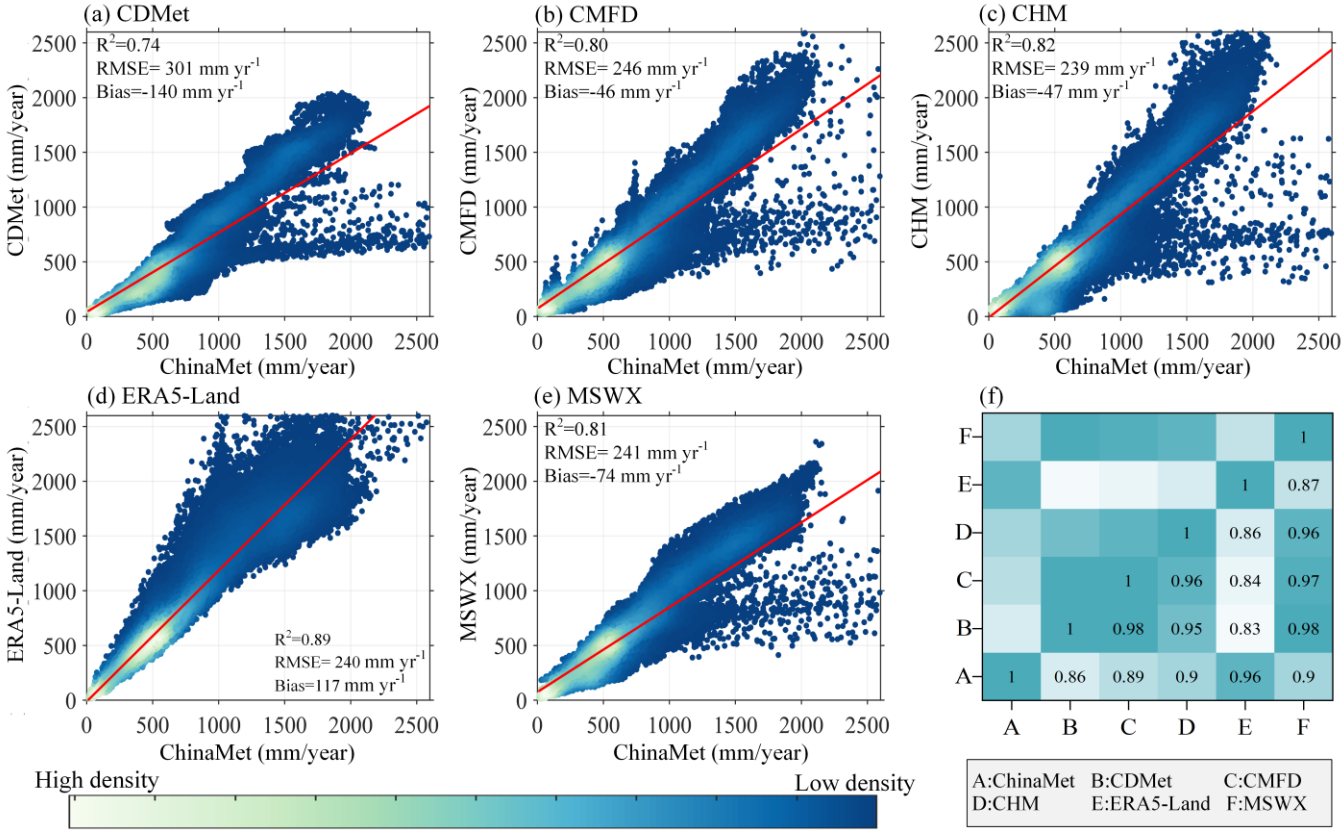


Figure 8. Comparison of multiyear mean annual precipitation between ChinaMet and five other precipitation products during 2000–2018: **(a–e)** scatterplots and **(f)** correlation heatmap.

To further evaluate the precipitation-estimation performance of ChinaMet in high-elevation regions with complex terrain, we compared the spatial distributions of mean annual precipitation from seven precipitation products over the Qinghai-Tibet Plateau (QTP) for 2000 to 2018, as shown in Figure 9. TPHiPr, which was developed using observations from more than 9,000 stations across the region (Jiang et al., 2023b), was adopted as the reference dataset. It should be noted that TPHiPr and ChinaMet share some common input data sources. Therefore, this comparison is intended to assess the spatial consistency among different precipitation products over the QTP rather than to provide a completely independent accuracy assessment. ChinaMet shows the closest agreement with TPHiPr, followed by ERA5-Land, with CC of 0.93 and 0.92, respectively. This is expected because TPHiPr was developed based on ERA5-Land, and ERA5-Land was also incorporated into ChinaMet. In contrast, CDMet and MSWX exhibit a pronounced dry bias, with annual precipitation generally ranging from 100 to 600 mm yr^{-1}, resulting in an underrepresentation of the high-precipitation regions in the southeastern QTP. Overall, ChinaMet shows relatively strong spatial consistency with TPHiPr over the QTP compared with the other evaluated products, where complex terrain and sparse observations pose substantial challenges to precipitation mapping.

https://doi.org/10.5194/essd-2026-704
Preprint. Discussion started: 16 November 2026
© Author(s) 2026. CC BY 4.0 License.

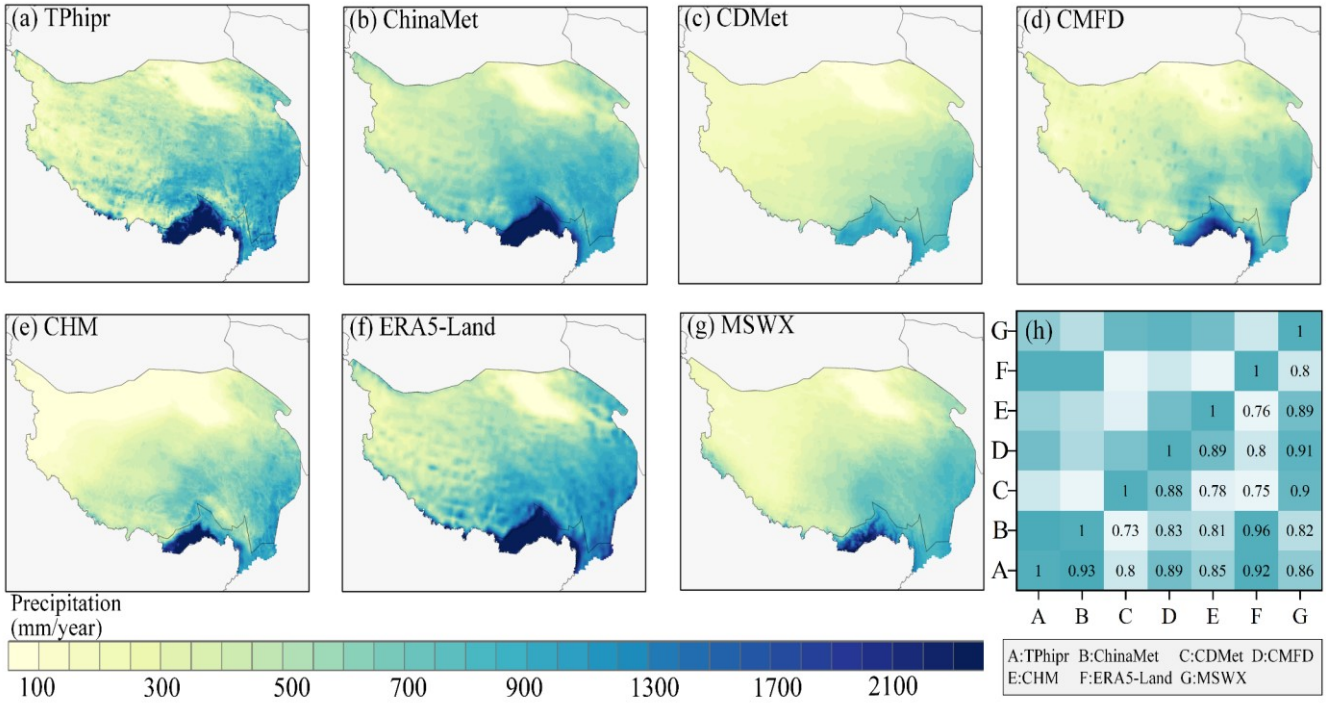


Figure 9. Spatial distributions of multiyear mean annual precipitation from seven precipitation products over the Qinghai–Tibet Plateau during 2000–2018, with TPHipr used as the reference.

Figure 10 shows the spatial distributions of mean annual air temperature from ChinaMet and five other temperature products for the period from 2000 to 2018. Overall, ChinaMet exhibits a spatial pattern consistent with CDMet, CMFD, CDAT, ERA5-Land, and MSWX across mainland China. Air temperature generally decreases from south to north, with values below 8 °C occurring mainly in northern China and high-elevation regions, whereas areas with mean annual temperatures above 20 °C are concentrated in southern China. This pattern is consistent with the combined influences of latitude and topography and accurately represents the temperature gradient from coastal to inland regions. Similar spatial patterns are also evident in the mean annual maximum and minimum air temperatures derived from ChinaMet, as shown in Supplementary Figure S2 and Figure S3. ChinaMet and CDMet exhibit relatively large differences over the Qinghai-Tibet Plateau. The observed mean annual temperature at the station locations, M.o, is 13.87 °C, whereas the corresponding product-derived values, M.c, are 13.79 °C for ChinaMet and 14.24 °C for CDMet. This discrepancy is mainly attributable to the pronounced warm bias of CDMet over the QTP. Figure 11 presents scatter-density plots comparing the mean annual air temperature from ChinaMet with those from the other five products. On average, the correlation coefficient between ChinaMet and the five products is 0.97. ChinaMet agrees most closely with ERA5-Land, with CC=0.99 and Bias = -0.48 °C. This strong agreement is expected because ERA5-Land is incorporated into the ChinaMet merging framework, and the virtual stations used in data-sparse regions are also primarily derived from ERA5-Land, allowing ChinaMet to retain much of its spatial heterogeneity

https://doi.org/10.5194/essd-2026-704
Preprint. Discussion started: 16 November 2026
© Author(s) 2026. CC BY 4.0 License.

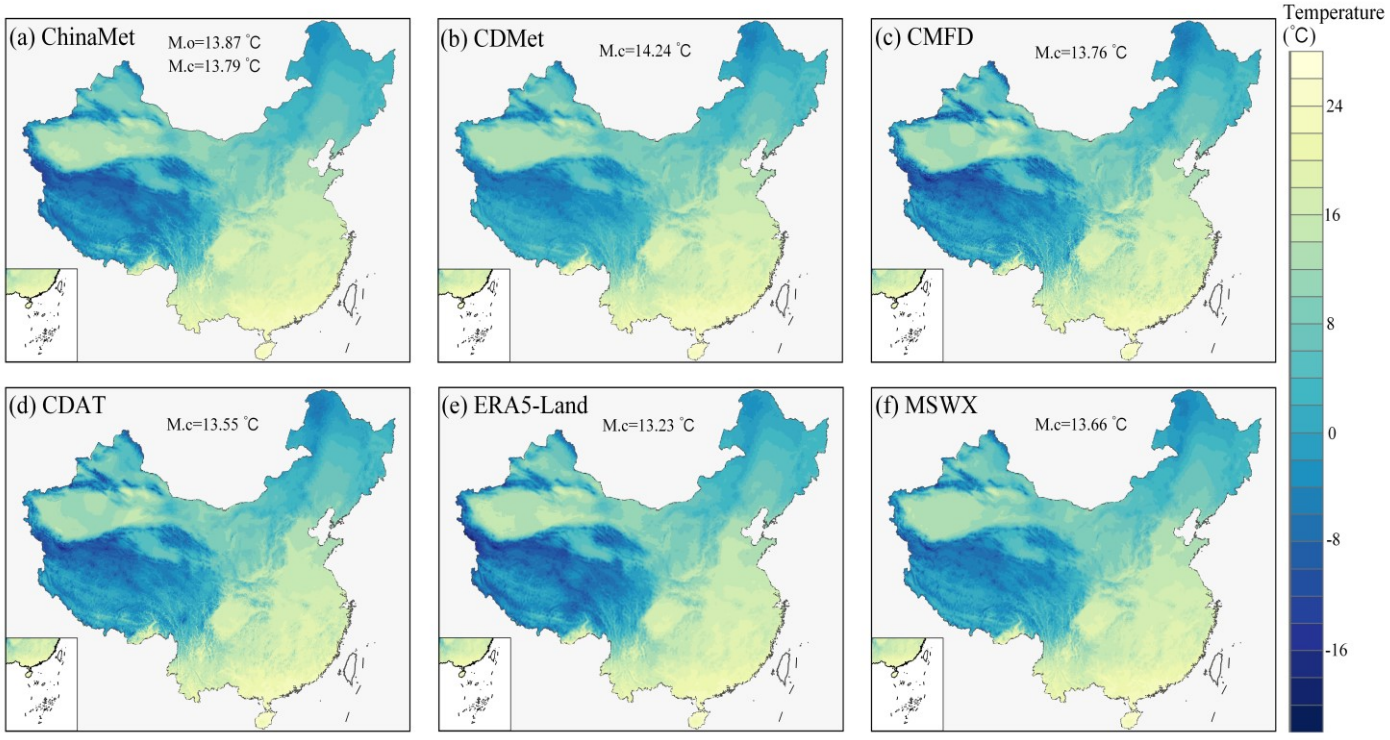


Figure 10. Spatial distributions of multiyear mean air temperature from six products during 2000–2018.

https://doi.org/10.5194/essd-2026-704
Preprint. Discussion started: 16 November 2026
© Author(s) 2026. CC BY 4.0 License.

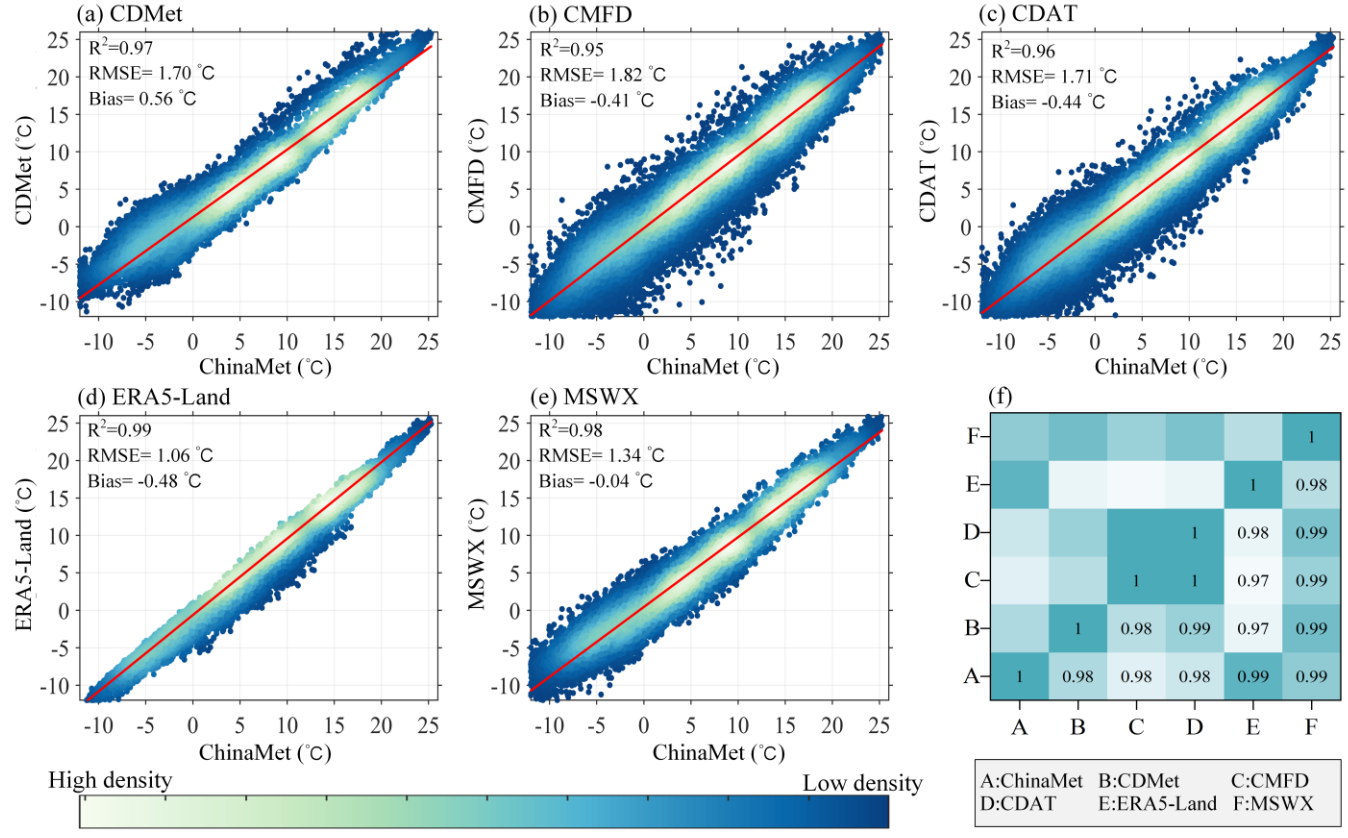


Figure 11. Comparison of multiyear mean air temperature between ChinaMet and five other products during 2000–2018: **(a–e)** scatterplots and **(f)** correlation heatmap.

Based on the high-resolution meteorological variables, two potential evapotranspiration datasets, ChinaMet-petPM and ChinaMet-petHG, were developed using the Penman-Monteith (PM) and Hargreaves (HG) methods, respectively. Supplementary Figure S4 shows the spatial distributions of six potential evapotranspiration (PET) products over mainland China from 2000 to 2018. PET-Peng is a previously published monthly evapotranspiration dataset developed by (Peng et al., 2019). ChinaMet-petHG exhibits spatial patterns consistent with those of PET-Peng and GLEAM, capturing the climatic gradient characterized by high PET in the arid regions of northwestern China and low PET over the Qinghai-Tibet Plateau and the cold regions of northeastern China. In contrast, ERA5 displays spatially discontinuous and anomalous patches over the complex terrain of western China. At the regional scale, ChinaMet-petPM shows pronounced overestimation over the central Qinghai-Tibet Plateau. This overestimation is mainly attributable to the high sensitivity of the PM equation to systematic biases in aerodynamic variables, particularly wind speed and vapor pressure deficit, in high-elevation regions with limited observations. Overall, ChinaMet-petHG exhibits spatial patterns broadly consistent with those of the reference PET products while retaining detailed terrain-related spatial variability, suggesting its potential utility for regional water-resources and ecohydrological applications.

https://doi.org/10.5194/essd-2026-704
Preprint. Discussion started: 16 November 2026
© Author(s) 2026. CC BY 4.0 License.


We also compared the spatial distributions of mean relative humidity, surface pressure, and wind speed from ChinaMet and comparable products over the period from 2000 to 2018, as shown in Supplementary Figure S5, Figure S6, and Figure S7. For relative humidity, ChinaMet, CDMet, ERA5-Land, and MSWX all show an increasing gradient from northwestern China toward the southeastern coast. However, CDMet produces lower humidity values over northwestern China and the Qinghai-Tibet Plateau and shows a sharper transition between dry and humid regions. ERA5-Land and ChinaMet exhibit the smoothest humidity patterns near the Qinling Mountains, the Huai River, and the Sichuan Basin. All products show highly consistent spatial patterns of surface pressure, with values increasing from the low-pressure region over the Qinghai-Tibet Plateau toward the southeastern coast. For near-surface wind speed, ChinaMet shows spatial patterns similar to those of CDMet and ERA5-Land, with relatively high wind speeds over northwestern China and the plateau regions and lower values over southeastern China. CMFD exhibits spatial discontinuities and anomalously high values in some regions, with wind speeds exceeding 4.9 m/s, possibly because the interpolation is constrained by the spatial distribution of stations. MSWX generally produces higher wind speeds, ranging from approximately 2.5 to 5.3 m/s, and shows a pronounced terrain-enhancement effect over the Qinghai-Tibet Plateau and northwestern China, resulting in a substantially larger extent of high-wind-speed regions. Overall, the relative humidity and wind-speed patterns of ChinaMet agree closely with those of ERA5-Land and CDMet, while its surface-pressure distribution is consistent with all evaluated products.

4.3. Uncertainty analysis of ChinaMet

Figure 12 and Figure 13 present the spatial distributions of the TCH-derived absolute uncertainty estimates for six meteorological products during 2000–2018. Overall, precipitation products exhibit larger uncertainty estimates than mean air temperature products, particularly over regions with complex terrain and strong moisture transport. For precipitation (Figure 12), ChinaMet exhibits the lowest spatially averaged TCH-derived absolute uncertainty estimate, with a mean value of 8.2 mm month^{-1}. CHM and MSWX follow with uncertainty estimates of 9.9 and 10.8 mm month^{-1}, respectively. CMFD and ERA5-Land show substantially higher uncertainty estimates of 17.7 and 16.5 mm month^{-1}, respectively, particularly over the Qinghai–Tibetan Plateau and the southeastern coastal regions. For mean air temperature (Figure 13), ChinaMet also exhibits the lowest spatially averaged TCH-derived uncertainty estimate, with a mean value of 0.36 °C. CDMet and MSWX rank second, with uncertainty estimates of 0.46 and 0.45 °C, respectively. ERA5-Land has the highest spatially averaged uncertainty estimate (0.68 °C), with relatively large values occurring over regions with complex terrain, including the Qinghai–Tibetan Plateau and the Tarim Basin. Overall, ChinaMet exhibits the lowest TCH-derived uncertainty estimates among the evaluated products for both precipitation and mean air temperature. These results indicate a lower estimated error standard deviation within the TCH framework. Because several products share common observations or reanalysis information, the TCH-derived uncertainty estimates should be interpreted as relative measures of uncertainty rather than absolute measures of product accuracy.

https://doi.org/10.5194/essd-2026-704
Preprint. Discussion started: 16 November 2026
© Author(s) 2026. CC BY 4.0 License.

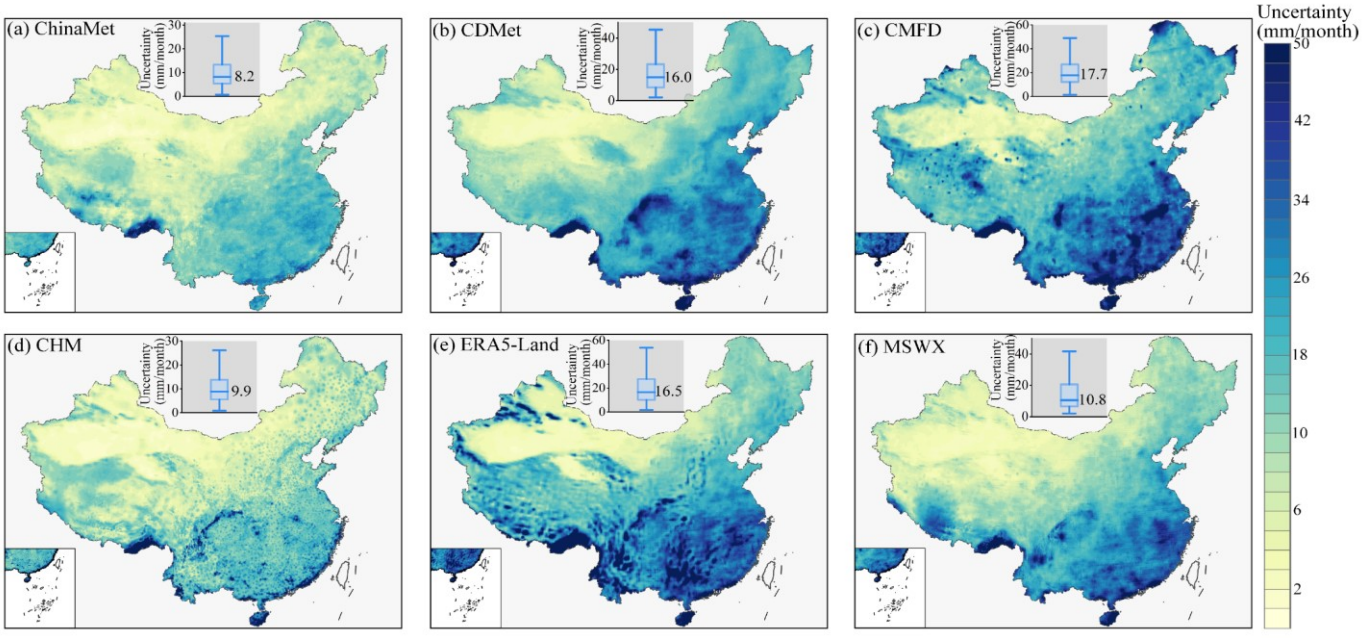


Figure 12. Spatial distributions of TCH-derived absolute uncertainty estimates for monthly precipitation from six products during 2000–2018.

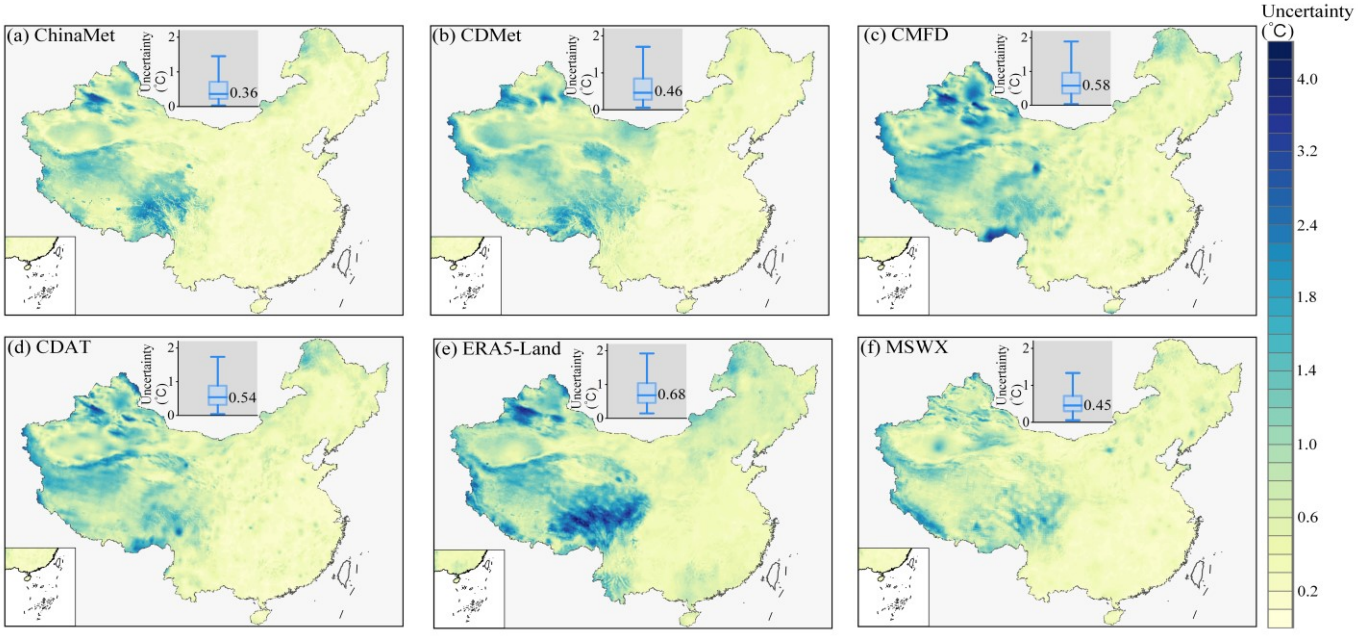


Figure 13. Spatial distributions of TCH-derived absolute uncertainty estimates for monthly mean air temperature from six products during 2000–2018.

https://doi.org/10.5194/essd-2026-704
Preprint. Discussion started: 16 November 2026
© Author(s) 2026. CC BY 4.0 License.



5 Discussion

5.1 Importance and uncertainty of using virtual stations

The virtual-station approach was introduced to improve the quality of ChinaMet in regions with sparse or absent ground observations. Candidate virtual stations were identified using a 0.75° grid. A grid cell was designated as a virtual-station location when it contained no observational station and no station was present within an additional 0.5° neighbourhood. To maintain consistency among virtual observations, ERA5-Land was used as the common reference dataset. This approach was intended to reduce unstable estimates over regions with complex terrain. As shown in Supplementary Figure S8, the spatial distributions of mean annual precipitation and air temperature from 2000 to 2018 generated without virtual stations exhibited pronounced underestimation over the Qinghai-Tibet Plateau (QTP). In particular, mean annual precipitation over much of the QTP ranged from only 300 to 700 mm/year, while the estimated mean annual air temperature reached a minimum of approximately -5 °C. The resulting spatial patterns were inconsistent with the expected regional climatic characteristics. This problem was primarily attributable to the limited station coverage over the QTP, where only approximately 5% of the stations used in this study were located, making it difficult to represent the strong spatial heterogeneity of this region. Moreover, ChinaMet generated without virtual stations systematically underestimated the precipitation statistics reported in the national water resources bulletins, particularly after 2000, when the estimated annual accumulated precipitation showed an unrealistic decline (Supplementary Figure S9). The introduction of virtual stations therefore substantially reduced observational gaps and improved the regional representativeness of the meteorological estimates. (Thiemig et al., 2022) similarly demonstrated that incorporating grid cells as virtual stations in observation-sparse regions can compensate for insufficient station information and improve the quality of the resulting data products.

Nevertheless, the use of virtual stations inevitably introduces additional uncertainty, particularly over the QTP. Most virtual stations were located in this region, where ERA5-Land generally produces relatively high precipitation and air temperature estimates. Consequently, ChinaMet may become overly dependent on ERA5-Land in data-sparse areas, creating a risk of propagating or amplifying its biases. As shown in Figure 9 and Figure 12, ERA5-Land estimates annual precipitation of approximately 1,500 mm year−1 over much of the southeastern QTP, substantially higher than the range of approximately 700 to 1,000 mm/year indicated by the other precipitation products. ERA5-Land also exhibits the highest monthly uncertainty in this region, ranging from approximately 28 to 45 mm/month. Users should therefore exercise particular caution when applying ChinaMet over the QTP and consider the potential influence of ERA5-Land-derived virtual stations.

5.2 Spatial trend of precipitation

In recent years, increasing attention has been given to the possible northward migration of precipitation isohyets across China. Some studies have suggested that precipitation has increased in the arid regions of northern China and that the national

https://doi.org/10.5194/essd-2026-704
Preprint. Discussion started: 16 November 2026
© Author(s) 2026. CC BY 4.0 License.


hydroclimatic pattern is undergoing a phase of adjustment. However, the magnitude and even the direction of this potential shift vary substantially among meteorological datasets, resulting in considerable scientific debate. A systematic spatial assessment based on multiple data sources and precipitation isohyets representing different climatic zones is still lacking. To address this issue, we compared the long-term evolution of the 200, 400, and 800 mm precipitation isohyets from 1981 to 2018 using five precipitation products, as shown in Supplementary Figure S10 and Table S2. The results indicate that the 200 and 400 mm isohyets, which broadly represent arid and semi-arid climatic boundaries, exhibit some degree of northward migration. In contrast, the 800 mm isohyet, representing the boundary of the humid region in southern China, does not show a consistent northward shift. In the latitudinal direction, ChinaMet, CMFD, ERA5-Land, and MSWX all indicate a northward displacement of the 200 and 400 mm isohyets to varying degrees. Although the trends are generally weak, with slope values below 0.2, they provide preliminary evidence that the boundaries of arid and semi-arid climatic regions may be shifting northward. By contrast, the 800 mm isohyet does not display a consistent migration pattern. Its estimated slope and P value differ substantially among the products, which is a major source of the ongoing debate regarding the northward shift of precipitation zones. The longitudinal migration of the three isohyets is similarly inconsistent. In some products, the 200 and 800 mm isohyets even move in opposite directions. These differences suggest pronounced spatial heterogeneity in regional responses to climate change and highlight the need to consider local topography, atmospheric moisture-transport pathways, and human activities when interpreting isohyet migration. One important cause of the disagreement among products is their inconsistent precipitation estimates over the humid regions of southern China. For example, ERA5-Land exhibits a pronounced systematic wet bias over southern and southwestern China, which directly affects the identification of the actual migration path of high-precipitation isohyets. It should also be noted that the present analysis ends in 2018. In recent years, particularly after 2020, intense extreme precipitation events have occurred frequently across many parts of China, and annual accumulated precipitation in some regions has substantially exceeded historical averages. The anomalously high precipitation observed around 2025 may indicate that the spatial distribution of precipitation across China is entering another phase of adjustment. Future studies should therefore extend the data record to 2023–2025 to reassess the migration of precipitation isohyets under the increasing occurrence of extreme climate events.

6 Data availability

The ChinaMet dataset is publicly available from the National Cryosphere Desert Data Center at https://doi.org/10.12072/ncdc.nieer.db6722.2025 (Zhang et al., 2025). It provides daily, monthly, and annual meteorological fields for China from 1980 to 2024 at spatial resolutions of 0.1° and 0.01°. The dataset includes precipitation, 2 m mean air temperature, daily maximum and minimum air temperature, 10 m wind speed, relative humidity, surface pressure, and potential evapotranspiration. Two estimates of potential evapotranspiration are provided, calculated using the Hargreaves and Penman–Monteith methods. All data are distributed in NetCDF format and organized by spatial resolution, meteorological variable, and temporal scale.

https://doi.org/10.5194/essd-2026-704
Preprint. Discussion started: 16 November 2026
© Author(s) 2026. CC BY 4.0 License.

Open Access Earth System Science Data Discussions

7 Conclusions

This study developed ChinaMet, a multisource integrated, high-resolution, multi-variable meteorological forcing dataset for China. ChinaMet integrates observations from more than 2,300 meteorological stations with satellite products, reanalysis data, and auxiliary geographic information to provide daily, monthly, and annual meteorological fields at 0.1° and 0.01° spatial resolutions for 1980–2024. The dataset includes precipitation, 2 m mean air temperature, daily maximum and minimum air temperature, 10 m wind speed, relative humidity, surface pressure, and potential evapotranspiration. By combining random forest-based multisource merging with climatologically aided downscaling, the proposed merging–downscaling framework substantially improves computational efficiency while retaining accuracy comparable to direct high-resolution merging.

Comprehensive evaluation against station observations, water resources bulletin statistics, national precipitation records, and widely used meteorological products demonstrates that ChinaMet reliably captures the major spatial gradients and temporal variability of meteorological conditions across China. ChinaMet performs particularly well for precipitation, showing close agreement with station-based annual precipitation and the strongest consistency with prefecture-level water resources bulletin statistics among the evaluated products. The Three-Cornered Hat analysis further indicates low monthly uncertainty for both precipitation and mean air temperature.

The introduction of ERA5-Land-derived virtual stations improves spatial stability and reduces extrapolation uncertainty in observation-sparse regions, particularly over the Tibetan Plateau and western China. However, estimates in these regions may retain some dependence on the ERA5-Land background field, especially where ground observations are extremely sparse. Users should therefore exercise caution when applying ChinaMet in high-elevation and poorly observed regions. Overall, ChinaMet provides a spatially detailed, temporally continuous, and internally consistent meteorological forcing dataset for hydrological modelling, ecological analysis, agricultural assessment, and climate-change studies across China.

Author contributions

YH carried out the experiments, analysed the results, and prepared the manuscript. LZ conceived the study, supervised the research, and reviewed and edited the manuscript. YZ provided technical support and contributed to data analysis and validation. TC contributed to the interpretation of the results and reviewed and edited the manuscript. All authors contributed to the discussion of the results and approved the final manuscript.

Competing interests

The authors declare that they have no conflict of interest.

https://doi.org/10.5194/essd-2026-704
Preprint. Discussion started: 16 November 2026
© Author(s) 2026. CC BY 4.0 License.



Open Access Earth System Science Data Discussions

Acknowledgements

This study is supported by the National Natural Science Foundation of China (42271286), the Youth Innovation Promotion Association of Chinese Academy of Sciences (2023454), and Key Research Program of Gansu Province (23ZDKA0004).

References

Amjad, M., Yilmaz, M. T., Yucel, I., and Yilmaz, K. K.: Performance evaluation of satellite- and model-based precipitation products over varying climate and complex topography, Journal of Hydrology, 584, 124707, 10.1016/j.jhydrol.2020.124707, 2020.

Beck, H. E., Van Dijk, A. I. J. M., Larraondo, P. R., McVicar, T. R., Pan, M., Dutra, E., and Miralles, D. G.: MSWX: Global 3-Hourly 0.1° Bias-Corrected Meteorological Data Including Near-Real-Time Updates and Forecast Ensembles, Bulletin of the American Meteorological Society, 103, E710-E732, 10.1175/BAMS-D-21-0145.1, 2022.

Beck, H. E., Wood, E. F., McVicar, T. R., Zambrano-Bigiarini, M., Alvarez-Garreton, C., Baez-Villanueva, O. M., Sheffield, J., and Karger, D. N.: Bias Correction of Global High-Resolution Precipitation Climatologies Using Streamflow Observations from 9372 Catchments, Journal of Climate, 33, 1299-1315, 10.1175/JCLI-D-19-0332.1, 2020.

Brocca, L., Filippucci, P., Hahn, S., Ciabatta, L., Massari, C., Camici, S., Schüller, L., Bojkov, B., and Wagner, W.: SM2RAIN–ASCAT (2007–2018): global daily satellite rainfall data from ASCAT soil moisture observations, Earth System Science Data, 11, 1583-1601, 10.5194/essd-11-1583-2019, 2019.

Ding, Y. and Peng, S.: Spatiotemporal change and attribution of potential evapotranspiration over China from 1901 to 2100, Theoretical and Applied Climatology, 145, 79-94, 10.1007/s00704-021-03625-w, 2021.

Ferreira, V. G., Montecino, H. D. C., Yakubu, C. I., and Heck, B.: Uncertainties of the Gravity Recovery and Climate Experiment time-variable gravity-field solutions based on three-cornered hat method, Journal of Applied Remote Sensing, 10, 015015, 10.1117/1.JRS.10.015015, 2016.

Fick, S. E. and Hijmans, R. J.: WorldClim 2: new 1-km spatial resolution climate surfaces for global land areas, International Journal of Climatology, 37, 4302-4315, 10.1002/joc.5086, 2017.

Funk, C., Peterson, P., Landsfeld, M., Pedreros, D., Verdin, J., Shukla, S., Husak, G., Rowland, J., Harrison, L., Hoell, A., and Michaelsen, J.: The climate hazards infrared precipitation with stations—a new environmental record for monitoring extremes, Scientific Data, 2, 150066, 10.1038/sdata.2015.66, 2015.

Gelaro, R., McCarty, W., Suárez, M. J., Todling, R., Molod, A., Takacs, L., Randles, C. A., Darmenov, A., Bosilovich, M. G., Reichle, R., Wargan, K., Coy, L., Cullather, R., Draper, C., Akella, S., Buchard, V., Conaty, A., da Silva, A. M., Gu, W., Kim, G.-K., Koster, R., Lucchesi, R., Merkova, D., Nielsen, J. E., Partyka, G., Pawson, S., Putman, W., Rienecker, M., Schubert, S. D., Sienkiewicz, M., and Zhao, B.: The Modern-Era Retrospective Analysis for Research and Applications, Version 2 (MERRA-2), Journal of Climate, 30, 5419-5454, https://doi.org/10.1175/JCLI-D-16-0758.1, 2017.

Gomis-Cebolla, J., Rattayova, V., Salazar-Galán, S., and Francés, F.: Evaluation of ERA5 and ERA5-Land reanalysis precipitation datasets over Spain (1951–2020), Atmospheric Research, 284, 106606, 10.1016/j.atmosres.2023.106606, 2023.

Gupta, H. V., Kling, H., Yilmaz, K. K., and Martinez, G. F.: Decomposition of the mean squared error and NSE performance criteria: Implications for improving hydrological modelling, Journal of Hydrology, 377, 80-91, 10.1016/j.jhydrol.2009.08.003, 2009.

He, J., Yang, K., Tang, W., Lu, H., Qin, J., Chen, Y., and Li, X.: The first high-resolution meteorological forcing dataset for land process studies over China, Scientific Data, 7, 25, 10.1038/s41597-020-0369-y, 2020.

Hersbach, H., Bell, B., Berrisford, P., Hirahara, S., Horányi, A., Muñoz-Sabater, J., Nicolas, J., Peubey, C., Radu, R., Schepers, D., Simmons, A., Soci, C., Abdalla, S., Abellan, X., Balsamo, G., Bechtold, P., Biavati, G., Bidlot, J., Bonavita, M., Chiara, G., Dahlgren, P., Dee, D., Diamantakis, M., Dragani, R., Flemming, J., Forbes, R., Fuentes, M., Geer, A., Haimberger, L., Healy, S., Hogan, R. J., Hólm, E., Janisková, M., Keeley, S., Laloyaux, P., Lopez, P., Lupu, C., Radnoti, G., Rosnay, P., Rozum, I., Vamborg, F., Villaume, S., and Thépaut, J. N.: The ERA5 global reanalysis,

https://doi.org/10.5194/essd-2026-704
Preprint. Discussion started: 16 November 2026
© Author(s) 2026. CC BY 4.0 License.



Quarterly Journal of the Royal Meteorological Society, 146, 1999-2049, 10.1002/qj.3803, 2020.

Hofstra, N., Haylock, M., New, M., Jones, P., and Frei, C.: Comparison of six methods for the interpolation of daily, European climate data, Journal of Geophysical Research: Atmospheres, 113, 2008JD010100, 10.1029/2008JD010100, 2008.

Hu, Y. and Zhang, L.: Added value of merging techniques in precipitation estimates relative to gauge-interpolation algorithms of varying complexity, Journal of Hydrology, 645, 132214, 10.1016/j.jhydrol.2024.132214, 2024.

Hu, Y., Zhang, L., Zhao, Y., and Che, T.: ChinaMet: A multisource integrated high-resolution multi-variable meteorological dataset for China, 10.5281/ZENODO.14580706, 2024.

Huffman, G. J., Bolvin, D. T., Braithwaite, D., Hsu, K.-L., Joyce, R. J., Kidd, C., Nelkin, E. J., Sorooshian, S., Stocker, E. F., Tan, J., Wolff, D. B., and Xie, P.: Integrated Multi-satellite Retrievals for the Global Precipitation Measurement (GPM) Mission (IMERG), in: Satellite Precipitation Measurement: Volume 1, edited by: Levizzani, V., Kidd, C., Kirschbaum, D. B., Kummerow, C. D., Nakamura, K., and Turk, F. J., Advances in Global Change Research, Springer International Publishing, Cham, 343-353, 2020.

Jiang, Q., Li, W., Fan, Z., He, X., Sun, W., Chen, S., Wen, J., Gao, J., and Wang, J.: Evaluation of the ERA5 reanalysis precipitation dataset over Chinese Mainland, Journal of Hydrology, 595, 125660, 10.1016/j.jhydrol.2020.125660, 2021.

Jiang, S.-h., Wei, L.-y., Ren, L.-l., Zhang, L.-q., Wang, M.-h., and Cui, H.: Evaluation of IMERG, TMPA, ERA5, and CPC precipitation products over mainland China: Spatiotemporal patterns and extremes, Water Science and Engineering, 16, 45-56, 10.1016/j.wse.2022.05.001, 2023a.

Jiang, Y., Yang, K., Qi, Y., Zhou, X., He, J., Lu, H., Li, X., Chen, Y., Li, X., Zhou, B., Mamtimin, A., Shao, C., Ma, X., Tian, J., and Zhou, J.: TPHiPr: a long-term (1979–2020) high-accuracy precipitation dataset (1⁄30°, daily) for the Third Pole region based on high-resolution atmospheric modeling and dense observations, Earth System Science Data, 15, 621-638, 10.5194/essd-15-621-2023, 2023b.

Kobayashi, S., Ota, Y., Harada, Y., Ebita, A., Moriya, M., Onoda, H., Onogi, K., Kamahori, H., Kobayashi, C., Endo, H., Miyaoka, K., and Takahashi, K.: The JRA-55 Reanalysis: General Specifications and Basic Characteristics, Journal of the Meteorological Society of Japan. Ser. II, 93, 5-48, 10.2151/jmsj.2015-001, 2015.

Mankin, K. R., Mehan, S., Green, T. R., and Barnard, D. M.: Review of gridded climate products and their use in hydrological analyses reveals overlaps, gaps, and the need for a more objective approach to selecting model forcing datasets, Hydrology and Earth System Sciences, 29, 85-108, 10.5194/hess-29-85-2025, 2025.

Muñoz-Sabater, J., Dutra, E., Agustí-Panareda, A., Albergel, C., Arduini, G., Balsamo, G., Boussetta, S., Choulga, M., Harrigan, S., Hersbach, H., Martens, B., Miralles, D. G., Piles, M., Rodríguez-Fernández, N. J., Zsoter, E., Buontempo, C., and Thépaut, J.-N.: ERA5-Land: a state-of-the-art global reanalysis dataset for land applications, Earth System Science Data, 13, 4349-4383, 10.5194/essd-13-4349-2021, 2021.

Peng, S., Ding, Y., Liu, W., and Li, Z.: 1 km monthly temperature and precipitation dataset for China from 1901 to 2017, Earth System Science Data, 11, 1931-1946, 10.5194/essd-11-1931-2019, 2019.

Sjoberg, J. P., Anthes, R. A., and Rieckh, T.: The Three-Cornered Hat Method for Estimating Error Variances of Three or More Atmospheric Datasets. Part I: Overview and Evaluation, Journal of Atmospheric and Oceanic Technology, 38, 555-572, 10.1175/JTECH-D-19-0217.1, 2021.

Stahl, K., Moore, R. D., Floyer, J. A., Asplin, M. G., and McKendry, I. G.: Comparison of approaches for spatial interpolation of daily air temperature in a large region with complex topography and highly variable station density, Agricultural and Forest Meteorology, 139, 224-236, 10.1016/j.agrformet.2006.07.004, 2006.

Tang, G., Clark, M. P., and Papalexiou, S. M.: EM-Earth: The Ensemble Meteorological Dataset for Planet Earth, Bulletin of the American Meteorological Society, 103, E996-E1018, 10.1175/BAMS-D-21-0106.1, 2022.

Thiemig, V., Gomes, G. N., Skøien, J. O., Ziese, M., Rauthe-Schöch, A., Rustemeier, E., Rehfeldt, K., Walawender, J. P., Kolbe, C., Pichon, D., Schweim, C., and Salamon, P.: EMO-5: a high-resolution multi-variable gridded meteorological dataset for Europe, Earth System Science Data, 14, 3249-3272, 10.5194/essd-14-3249-2022, 2022.

Thornton, P. E., Running, S. W., and White, M. A.: Generating surfaces of daily meteorological variables over large regions of complex terrain, Journal of Hydrology, 190, 214-251, 10.1016/S0022-1694(96)03128-9, 1997.

Wan, Z., Hook, S., and Hulley, G.: MODIS/Terra Land Surface Temperature/Emissivity Daily L3 Global 1km SIN Grid V061, 10.5067/MODIS/MOD11A1.061, 2021.

Willmott, C. J. and Robeson, S. M.: Climatologically aided interpolation (CAI) of terrestrial air temperature, International

https://doi.org/10.5194/essd-2026-704
Preprint. Discussion started: 16 November 2026
© Author(s) 2026. CC BY 4.0 License.



Journal of Climatology, 15, 221-229, 10.1002/joc.3370150207, 1995.

Xia, Y., Sheffield, J., Ek, M. B., Dong, J., Chaney, N., Wei, H., Meng, J., and Wood, E. F.: Evaluation of multi-model simulated soil moisture in NLDAS-2, Journal of Hydrology, 512, 107-125, 10.1016/j.jhydrol.2014.02.027, 2014.

Xu, T., Guo, Z., Xia, Y., Ferreira, V. G., Liu, S., Wang, K., Yao, Y., Zhang, X., and Zhao, C.: Evaluation of twelve evapotranspiration products from machine learning, remote sensing and land surface models over conterminous United States, Journal of Hydrology, 578, 124105, 10.1016/j.jhydrol.2019.124105, 2019.

Yan, X., Zhang, B., Yao, Y., Yang, Y., Li, J., and Ran, Q.: GRACE and land surface models reveal severe drought in eastern China in 2019, Journal of Hydrology, 601, 126640, 10.1016/j.jhydrol.2021.126640, 2021.

Yu, C., Shao, H., Hu, D., Liu, G., and Dai, X.: Merging precipitation scheme design for improving the accuracy of regional precipitation products by machine learning and geographical deviation correction, Journal of Hydrology, 620, 129560, 10.1016/j.jhydrol.2023.129560, 2023.

Zhang, L., Hu, Y., Zhao, Y., and Che, T.: ChinaMet: A High-resolution Multi-element Meteorological Driving Dataset for China via Multi-source Data Fusion [Dataset], National Cryosphere Desert Data Center, https://doi.org/10.12072/ncdc.nieer.db6722.2025, 2025.

Zhang, L., Li, X., Zheng, D., Zhang, K., Ma, Q., Zhao, Y., and Ge, Y.: Merging multiple satellite-based precipitation products and gauge observations using a novel double machine learning approach, Journal of Hydrology, 594, 125969, 10.1016/j.jhydrol.2021.125969, 2021.

Zhang, T., Liang, Z., Wang, H., Wang, J., Hu, Y., and Li, B.: Merging multisatellite precipitation products using stacking method and the censored-shifted gamma ensemble model output statistics in china's Beimiaoji basin, Journal of Hydrology, 618, 129263, 10.1016/j.jhydrol.2023.129263, 2023.

Zhao, T. and Yatagai, A.: Evaluation of TRMM 3B42 product using a new gauge-based analysis of daily precipitation over China: EVALUATION OF TRMM 3B42 PRODUCT OVER CHINA, International Journal of Climatology, 34, 2749-2762, 10.1002/joc.3872, 2014.